Canadian Science Publishing | Canadian Geotechnical Journal

Field investigation of shallow soft-soil highway subgrade treated by mass carbonation technology

Journal:	*Canadian Geotechnical Journal*
Manuscript ID	cgj-2020-0008.R1
Manuscript Type:	Article
Date Submitted by the Author:	18-Mar-2020
Complete List of Authors:	Liu, Songyu; Southeast University - Sipailou Campus Cai, Guang-Hua; Nanjing Forestry University, College of Civil Engineering; Southeast University, Institute of Geotechnical Engineering Du, Guang-Yin; Southeast University Wang, Liang; Southeast University Li, Jiang-Shan; Chinese Academy of Sciences, Institute of Rock and Soil Mechanics Qian, Xing-Chen; Southeast University
Keyword:	mass carbonation, reactive magnesia, soft soil, field investigation, engineering properties
Is the invited manuscript for consideration in a Special Issue? :	Not applicable (regular submission)

Field investigation of shallow soft-soil highway subgrade treated by mass carbonation technology

Song-Yu Liu

Professor, Institute of Geotechnical Engineering, Jiangsu Key Laboratory of Urban Underground Engineering & Environmental Safety, Southeast University, Nanjing 211189, China. (E-mail: liusy@seu.edu.cn ORCID: 0000-0002-8135-3806)

Guang-Hua Cai*

Lecturer, School of Civil Engineering, Nanjing Forestry University, Nanjing 210037, China; Ph.D. Graduate, Southeast University, Nanjing 211189, China. (E-mail: ghcai@njfu.edu.cn; caiguanghua@seu.edu.cn ORCID: 0000-0003-1667-1733. *Corresponding author)

Guang-Yin Du

Associate Professor, Institute of Geotechnical Engineering, Southeast University, Nanjing 211189, China. (E-mail: guangyin@seu.edu.cn ORCID: 0000-0002-1253-5761)

Liang Wang

Master graduate, Institute of Geotechnical Engineering, Southeast University, Nanjing 211189, China. (E-mail: 925331835@qq.com ORCID: 0000-0003-3016-7058)

Jiang-Shan Li

Professor, Institute of Rock and Soil Mechanics, Chinese Academy of Sciences, Wuhan, 430071, China (E-mail: jsli@whrsm.ac.cn)

Xing-Chen Qian

Master graduate, Institute of Geotechnical Engineering, Southeast University, Nanjing 211189, China. (E-mail: clinext@163.com)

Revised version submitted for possible publication in

Canadian Geotechnical Journal

No. of Words: 7,348 (without Abstract, Acknowledgements and References)

No. of Tables: 5

No. of Figures: 16

Abstract: The innovative carbonation technique based on reactive MgO and CO_2 has been identified as an environmentally friendly and efficient method in the improvement of weak soils. Previous laboratory studies have indicated that carbonated MgO-admixed soils had significant improvement in mechanical properties. However, there are to date limited investigations on the soft-soil field application of this technique. In this study, a field trial was conducted to ascertain the feasibility of the MgO mass carbonation technique in improving shallow soft-soil subgrades. A series of field tests, including temperature, dynamic cone penetrometer and light weight deflectometer tests, were undertaken. The results indicated that compared to uncarbonated soil layers, there was 2-3 times increase in dynamic resilient moduli and soil resistances of carbonated MgO-admixed soils. The outcomes of this field investigation will contribute to the utilization of the combined stabilizer of MgO and CO_2 and the mass carbonation technology in subgrade improvement.

Keywords: mass carbonation, reactive magnesia, soft soil, field investigation, engineering properties

Introduction

Soft soils, prevalent in floodplains, deltas, coastal areas such as East China regions, are usually discouraged from direct use in engineering practices due to low strength and permeability as well as high water content and compressibility (Chian et al. 2016; Jiang et al. 2016). Such poor geotechnical characteristics make soft soils difficult to use in highway embankments and foundations through compacting, resulting in their excessive settlement and long consolidation time (Liu et al. 2012; Bo et al. 2015; Zhao et al. 2018). They give the highway subgrades low bearing capacity and make them susceptible to unacceptable differential settlements under any imposed traffic loading (Chakrabarti and Kodikara 2007; Han et al. 2007; Lu et al. 2019). To overcome these shortcomings, it is necessary to either replace unwanted soft soils with desirable soils or improve their mechanical properties using soil improvement techniques in geotechnical engineering practices (Chai et al. 2014; Han et al. 2007; Shen et al. 2013; Liu et al. 2012; Du et al. 2016; Jiang et al. 2016; Xia et al. 2019).

Soil improvement is the process of enhancing the engineering performance of weak soils through various methods such as physical, chemical, biological treatments and so forth (Bo et al. 2015; Arulrajah et al. 2012, 2016; Disfani et al. 2017; Du et al. 2016; Howayek et al. 2019). For the physical ground improvements, there were some shortcomings such as low efficiency and long treatment time in spite of the successful use of the vacuum preloading and electro-osmosis methods in improving dredged clay-slurry (Cai et al. 2018; Wang et al. 2016, 2018). The emerging bio-mediated technique, regarded as a potentially environmentally friendly improvement method, could improve the mechanical properties of sandy soils, but current studies demonstrated that it was difficult for this technique to treat large-area soft soils

due to its high economic cost and long time consumption (Hoang et al. 2019; Howayek et al. 2019; Liu et al. 2019; Zamani et al. 2019). But unlike the aforementioned methods, the popular chemical stabilization using cementitious binders such as lime and ordinary Portland cement (PC) was a well-established technique for soft ground improvement (Martin et al. 2012; Shen et al. 2013; Abiodun and Nalbantoglu 2015; Latifi et al. 2018).

Although previous studies have demonstrated that PC stabilization can effectively improve the geotechnical performance of soft soils, the environmental issues related to PC production made its application undesirable (Diniz et al. 2017; Zhang et al. 2020). These issues mainly included but were not limited to: (*i*) the energy-intensive nature of PC production (5000 MJ energy/t PC, calcining temperature > 1450°C); (*ii*) non-renewable resource consumption (1.5 t limestone and clay/t PC); (*iii*) significant CO_2 emissions (0.95 t CO_2 /t PC), NO_x (nitrogen oxide) emissions and particulate pollutions associated with industrial processes; and (*iv*) the generation of industrial waste materials and non-beneficial byproducts (Latifi et al. 2018; Zhang et al. 2019, 2020). The aforementioned concerns have led to a growing interest in exploring more-sustainable alternative additives with small environmental footprints and reasonable cost, which has further promoted the utilization of geopolymers and industrial byproducts (e.g., fly ash, slag, carbide slag and lignin) as well as low-carbon materials (e.g., MgO) (Liska et al. 2008; Horpibulsuk et al. 2012, 2013; Sukmak et al. 2013; Jiang et al. 2016; Yi et al. 2013*a*; Cai et al. 2020; Mozumder and Laskar 2015; Zhang et al. 2020). Geopolymers have been discovered to be good alternative binders generally manufactured from low-calcium high-aluminosilicate materials (e.g., fly ash and ground granulated blast slag (GGBS)) which could be activated in a highly alkaline medium

(Mozumder and Laskar 2015). Under an alkaline activator, geopolymers could lead to the cementation of soil particles through a three-phase chain of chemical multi-reaction called "geopolymerization" (Abdullah et al. 2020). Some studies addressed the use of alkaline materials (e.g., lime and carbide slag (CS)) to activate GGBS in soft clay stabilization, and indicated that the unconfined compressive strength of the optimum lime-GGBS and CS-GGBS stabilized clays was more than 1.7 times and twice that of the corresponding PC stabilized clays (Yi et al. 2015*a*, 2015*b*). Besides, the byproduct of CS could also be mixed with soft clay alone and reacted with clay minerals to improve the strength, stiffness and durability of the stabilized soil, demonstrating superior mechanical performance of CS-stabilized soil over lime-stabilized clay (Du et al. 2016; Kampala et al. 2013; Jiang et al. 2016).

In recent years, reactive MgO was chosen as a low-carbon soil stabilizer compared to PC, owing to low calcination temperature (~700-800°C), little energy consumption and reduced CO_2 emissions during its production process, as well as great potential in CO_2 absorption during the application process (Cai et al. 2015; Yi et al. 2013*a*, 2016). The carbonation of reactive MgO has consequently been employed as a sustainable and environmentally friendly technique in the improvement realms of weak soils compared to PC stabilization (Yi et al. 2013*a*, 2016; Liu et al. 2020). Numerous laboratory studies have proven that reactive MgO-admixed soils could complete accelerated carbonation under high-pressure CO_2 in a relatively short period (i.e., several hours), and thus have higher strength, modulus and density as well as increased soil durability compared to PC-stabilized soils (Yi et al. 2013*a*, 2013*b*, 2016; Cai et al. 2015, 2019*a*). The unconfined compressive strength of

MgO-carbonated sandy and silty soils (3-6 hours) was more than twice that of corresponding PC-stabilized soils (28 days) at the same dosage (Yi et al. 2013*a*, 2013*b*). This was mainly attributed to the carbonation products (e.g., nesquehonite, dypingite and hydromagesite) which resulted in the cementation of soil particles and the filling of pores (Unluer and Al-Tabbaa 2013, 2015; Yi et al. 2013a, 2016; Cai et al. 2015, 2019b). The geotechnical characteristics revealed above could well evaluate the viability of MgO-carbonated soils as a subgrade material.

Although there were numerous studies on the physical, mechanical and microstructural properties of carbonated MgO-admixed soils in recent years, previous studies only focused on small-scale laboratory settings. Little attention has been paid to the field trials of MgO-CO_2 carbonation technique in the treatment of soft highway subgrade and its effectiveness. The improvement of in-situ soft soils was usually implemented using either of the two principal methods: deep stabilization such as dry deep mixing (Fang et al. 2001; Martin and Bryan 2017) and mass stabilization (Jelistic and Leppanen 2003; Wheeler et al. 2017). For dry deep mixing, the installation depth of stabilized columns was far more than 5 m, and the treatment effect was greatly impacted by such factors as the shape of mixing blade, rotational speed, and velocity of penetration and retrieval of mixing equipment (Madhyannapu et al. 2010). In contrast, the mass stabilization was regarded as an efficient means for stabilizing large areas of shallow soft ground (< 5 m) (Jelistic and Leppanen 2003; Martin et al. 2012; Wheeler et al. 2017). Therefore, the present research attempted to treat the shallow soft-soil highway subgrade by employing the mass carbonation/stabilization method. The objective of this work was to investigate the mechanical performance of MgO-carbonated shallow highway

subgrades through several field tests including dynamic cone penetrometer and light weight deflectometer, and then to discuss the effectiveness and feasibility of this technique based on field results and microstructure analyses. Similarly, multi-scale observations would be helpful to understanding the controlling mechanisms of MgO-carbonated soils, to promoting the resource utilization of greenhouse CO_2 in geotechnical engineering, as well as to better applying the low-carbon and high-efficiency improvement technique to shallow highway subgrades.

Materials and Methodology

Site description

This section mainly introduced the field test location, its geological profile and geotechnical properties of muddy soil. The field trial was carried out on a Ramp Road (*K*4+690) along the Yichang (Yixing to Changxing) Highway. The test site was located at Zhangzhu town (119.61° E, 31.34° N) in Yixing, Jiangsu Province, China, as shown in **Fig. 1(a)**, and the field scene before treatment was shown in **Fig. 1(b)**. According to a static cone penetration test (ASTM 2016), the subsoil consisted of muddy soil (from 0.8 to 1.8 m deep), silty clay (from 1.8 to 4.0 m deep) and clay (from 4.0 to 6.5 m deep). The ground water level fluctuated between ~1.4 to 2 m below the ground surface.

The test site was a low-lying ditch with the perimeter of ~105 m, area of ~600 m^2, water depth of ~0.8 m and average mud depth of ~1.0 m. After the drainage and cleaning of debris and weeds, the muddy soil was sampled to measure the physical and chemical properties, and the seepage ditch was excavated to continuously reduce the water content until it was close to the liquid limit. After two weeks, the average water content was about 45% for the north part

of the ditch pond, and over 54% for the south part due to its lower ground surface. **Table 1** shows the testing results of physical and chemical properties of the muddy soil. The Atterberg limits, particle-size composition, classifications and specific gravity of the muddy soil were determined according to ASTM D4318 (ASTM 2010*a*), ASTM D422 (ASTM 2007*a*), ASTM D2487 (ASTM 2011*a*), and ASTM D854 (ASTM 2010*b*), respectively. The soil was classified as a low plasticity clay (*CL*) as per ASTM D2487 (ASTM 2011*a*). The pH of soil was measured by using a portable D-54 pH meter according to ASTM D4972 (ASTM 2007*b*), and the mixture solution used was composed of 2 mm-sieved dry soils (10 g) and deionized water (10 g). The X-ray fluorescence (XRF) analysis indicated that the muddy soil mainly contained 69.8% of silicon dioxide (SiO_2), 17.8% of aluminum oxide (Al_2O_3), 5.3% of ferric oxide (Fe_2O_3), 2.1% of potassium oxide (K_2O), 1.0% of magnesium oxide (MgO), and 1.1% of calcium oxide (CaO) (**Table 2**).

Materials

Considering the material cost, the heavy-burned MgO whose price was slightly cheaper than that of PC was chosen as the principal binder in this field study. This MgO was obtained from the industrial calcination (750-1000^{o}C) and trituration of magnesite from Dashiqiao, Liaoning Province, China. The MgO showed a light yellow color due to its high impurity and low activity. The physical properties of MgO are shown in **Table 1**. The specific gravity was determined as per ASTM D854 (ASTM 2010*b*) and the grain-size distribution of MgO was examined by using a laser particle size analyzer. To avoid hydration of MgO, the water-free kerosene was chosen as the dispersing medium in the two tests. The specific surface area of MgO was found to be 7.21 m^2/g using an ASAP2020 Physisorption Analyzer, and the activity

content was measured to be 62% based on the weight change during the hydration process. The chemical compositions of MgO were obtained from the XRF test, as listed in **Table 2**. To prevent MgO powder from deliquescence and caking, MgO was transported to the construction site in bags and stacked on the tarpaulins laid on the floor and then it was covered by a waterproof tent (**Fig. 2(a)**). Moreover, some essential auxiliary materials were also used including perforated PVC pipes, PE pipes, quick unions and high-pressure pipes with multiple pipelines for transportation of CO_2 gas with a concentration of 99.9% (**Fig. 2(b-e)**). The perforated PVC pipes (~1.0 m) were artificially made from the PVC line pipes with a length of 4.0 m and were then drilled at the interval of ~10 cm. The CO_2 gas was supplied by Yixing Shenniu Special Gases Co. Ltd. in Jiangsu province, China, and the weight of each tank was about 40 kg (**Fig. 2(f)**).

Mass carbonation equipment

Previous studies have shown that there was various mixing equipment used in the mass stabilization, such as deep soil mixing augers, road reclamation machineries, pulver mixers, high pressure jets, and power mixers attached to excavators (Wilk 2014; Wheeler et al. 2017). The construction system of mass carbonation used in this study was developed by Southeast University and Nanjing Luding Stirring Pile Special Technology Co. Ltd. The system mainly consisted of two parts: (*a*) a power mixer attached to an excavator, which can inject the binder at the point of mixing (**Fig. 3 (a)**); and (*b*) a pressure feeder system made up of a feed tank and a storage tank with a capacity of ~1.0 ton (**Fig. 3 (b)**). The effective combination of the two parts can transfer MgO powders from the tanks through a powder spraying pipe (or hose) to the power mixer (**Fig. 3 (a, b)**). Moreover, the attachments used for the binder feeder also

198 included an alternator and an air compressor (**Fig. 3 (c, d)**). All equipment and attachments
199 were connected according to the schematic configuration of the system (**Fig. 3 (e)**). The
200 power mixer attached to the excavator was mainly consisted of a supporting arm, a power
201 converter, an agitator arm with a length of ~3.0 m and two-directional mixing heads with a
202 diameter of 1.2 m. It was worth noting that the supporting arm and agitator arm can operate
203 vertically or at a certain angle.

204 **Mass carbonation treatment procedures**

205 About 10% (*w*/*w*) of the MgO dosage was adopted in this field study based on previous
206 laboratory studies, actual water content and subgrade capacity requirement. And the amount
207 of MgO powder was controlled by the number of storage tanks and the earth volume
208 measured by depth and area. **Figures 4** and **5** show the flow chart and field pictures of the
209 construction procedure for the mass carbonation treatment of MgO-admixed soft soils. The
210 pretreatments of drainage, cleaning and water reduction (below liquid limit) were performed
211 prior to the assembly and connection of the mass treatment system. After successive drainage
212 and in-situ soil levelling, MgO powders were first put into the feed tank and storage tank
213 successively, and then transferred into the specified site through hoses with the help of an air
214 compressor. Subsequently, the mass carbonation treatment was carried out by inserting the
215 power mixer head into the soft soil subgrade while injecting and mixing MgO powders (**Fig.**
216 **5(a)**). The excavator moved along the edge of the ditch pond, and its maximum working
217 radius was approximately 10 m. Under this condition, a circle movement of the excavator
218 along the ditch pond could achieve the complete mixing of the whole ditch pond. Repetitive
219 mixing was performed from the bottom to the surface of the soft soil layer until achieving the

220 homogeneity, and the treating depth corresponded to 0.8–1.2 m (**Fig. 5(b)**).

221 After mixing the whole site, the MgO-admixed soft soil was levelled again and
222 compacted slightly, and the drain was excavated again along the edge of the ditch pond to
223 avoid the accumulation of water (**Fig. 5(c)**). Subsequently, the perforated PVC pipes and
224 Pt100 thermal-resistance temperature sensors were inserted into the MgO-admixed soil layer
225 according to the arrangement diagram (**Fig. 6**). The PVC pipes were connected to the CO_2
226 tanks through the PE pipes and high-pressure pipes in turn (**Fig. 5(d, e)**), and then the
227 MgO-admixed soft soil site was covered with the sealing film to avoid CO_2 leakage. Finally,
228 the site was ready for CO_2 carbonation through adjusting the valve (**Fig. 5(f)**). To study the
229 effect of initial water content and ventilation condition on soil treatment, the treatment site
230 was divided into four zones for comparison (**Fig. 7(a)**), and the corresponding processing
231 characteristics for each zone were listed in **Table 3**.

232 **Field tests**

233 To assess the carbonation efficiency, the bearing capacity and compaction characteristics
234 of treated soils, the temperature was monitored by temperature sensors during the CO_2
235 ventilation, and the monitored data was recorded by a DT80 Datataker acquisition. Most of
236 temperature sensors were placed into the middle of the soil layer based on different distances
237 from one of PVC pipes, and the rest of sensors were placed on the upper soil layer for
238 comparison. Since the field experiment was conducted during the middle of January with the
239 average daily temperature of around 0°C, the ventilation time was selected between 9:00 AM
240 and 17:00 PM to reduce the effect of low ambient temperature on CO_2 transmission. The
241 convenient and inexpensive measurements of dynamic resilience modulus and dynamic cone

242 penetrometer were used in this study (Acar et al. 1991; Du et al. 2016; Xia et al. 2019), and
243 the detailed layouts of testing points in every zone were illustrated in **Fig. 7(b)**.

244 The dynamic resilience modulus, typically used to evaluate the compaction degree of
245 subsoils, was tested by light weight deflectometer (LWD) which was also referred to as a
246 portable falling-weight deflectometer, light drop weight tester and dynamic plate load test
247 (ASTM 2011*c*). The LWD was a portable device (ZFG3000 EVD) developed in Germany,
248 and it was especially suitable for measuring the coarse-grain or mixed soils with a diameter of
249 less than 63 mm. The LWD equipment was made up of a load application system and a data
250 collection system (Beaulieu et al. 2014). The load was applied on a circular plate using a mass
251 hammer, and the applied stress depended on the mass hammer itself, drop height, and the
252 radius of circular plate. The load duration was about 20 milliseconds, and the load applied on
253 the LWD was 7.07 kN. When the falling hammer hit the circular plate, the vertical
254 displacement between the subgrade soil and circular plate was generated under the effect of
255 impact load, and the corresponding pressure and settlement were recorded by the data
256 collection system. Finally, the dynamic resilience modulus was determined according to Eq.
257 (1):

258 $$E_{\mathrm{vd}} = \frac{2\pi p\delta(1-\mu^2)}{4l} \tag{1}$$

259 where E_{vd} was the dynamic resilience modulus (MPa); p was the maximum uniform load
260 measured by bearing plate (kPa); δ was the radius of bearing plate (150 mm); μ was the
261 poisson ratio of soil; and l was the maximum deflection of bearing plate (mm).

262 The dynamic cone penetrometer test was performed to determine the bearing capacity
263 properties of MgO-admixed soils before and after carbonation according to the China

standard described in JTG E60-2008 (China JTG 2008), which was basically consistent with ASTM D6951 (ASTM 2009). The dynamic cone penetrometer testing points were next to LWD points to avoid the effect of LWD's compaction on the bearing capacity. In this study, the dynamic cone penetrometer equipment was consisted of a 10-kg drop hammer, a penetration rod and a cone tip with 25-mm base diameter. The drop height of hammer was 500 mm, and the cone angle was 60°. The dynamic cone penetrometer testing results were normally expressed by the soil penetration resistance (R_s) and dynamic cone penetrometer index (DCPI, mm/blow), which could be calculated by the Eq. (2) and Eq. (3), respectively (Burnham 1997; Mohammadi et al. 2008; Du et al. 2016; Martin and Bryan 2017; Xia et al. 2019). Besides, the bearing capacity could be approximately calculated according to Eq. (4) (China NRA 2018):

$$R_s = W_s / P_d = mgh / P_d \tag{2}$$

$$\mathrm{DCPI} = \Delta D_p / \Delta N \tag{3}$$

$$p_u = 8N_{10} - 20 \tag{4}$$

where R_s was the soil penetration resistance (kN); W_s was the work done by the soil (J), P_d is the distance which the penetrometer travels through the soil layer (cm), m was the standard hammer mass, g was the gravity acceleration (9.8 m/s^2); h was the fall distance (50 cm); DCPI was the penetration depth per blow of the hammer (mm/blow); ΔD_p was the penetration depth (mm); ΔN was the number of blow at ΔD_p; p_u was the bearing capacity (kPa); and N_{10} was the penetration blow corresponding to 30 cm falling distance of cone tip.

After the field tests, some samples were collected using the ring cutter sampler to measure the shear strength parameters as well as physicochemical and microstructural

characteristics. Four samples obtained from the same point were scrapped and then subjected to direct shear tests under the vertical stress of 50, 100, 200 and 400 kPa (ASTM 2011*b*). After direct shear tests, a certain amount of broken soils were dried to determine the water content at 45°C, as the high temperature (above 50°C) may cause the bound water loss of nesquehonite (Unluer and Al-Tabbaa 2013, 2015). Additionally, the testing methods of specific gravity, Atterberg limits and classifications and soil pH were consistent with earlier statements (ASTM 2007, 2010*a*, 2010*b*, 2011*a*). To conduct X-ray diffraction (XRD) and scanning electron microscopy (SEM) tests, the fragments were first frozen by immersion in liquid nitrogen (boiling point of -195°C), and then placed into a freezing unit (-80°C) with a vacuum chamber for further drying. Subsequently, one piece of freeze-dried fragment was selected and coated with a gold layer, and then SEM-EDS tests were conducted by using a FEI Inspect F50 field emission scanning electron microscope. The other freeze-dried samples were further ground (< 75 μm) for the XRD test. The XRD test was carried out by employing a Science SmartLab (3) Intelligent X-ray diffractometer under Cu-Kα radiation (wavelength of 1.54059 Å) with an input voltage of 40 kV and a current of 30 mA, and it was scanned from 10° to 65° two theta at a scanning speed of 10 s/step (a step size of 0.02°).

Results and Analyses

Temperature

Figure 8 presents the variation in temperature of the MgO-stabilized soft soil layers during the CO_2 ventilation. The variation in temperature revealed the carbonation efficiency under different initial water contents, distances from PVC pipes and CO_2 ventilation time to a certain degree. As shown in **Fig. 8**, the temperature of MgO-stabilized soil (~20°C) was far

higher than the ambient temperature (~6°C) during the ventilation periods, which was attributed to the generation and accumulation of considerable amounts of heat during the hydration reaction of moist MgO-admixed soil under the plastic film (**Eq. (5)**). The similar temperatures of several zones before CO_2 ventilation indicated the similar hydration degree of MgO. During the CO_2 ventilation period, the temperature increased to the maximum value in the first 3 hours, and then tended to decrease after a steady period. The results could be explained by the fact that the carbonation of hydration product ($Mg(OH)_2$) with CO_2 was an exothermic reaction (Eq. (6)) (Yi et al. 2016; Cai et al. 2019*b*). Some other results can also be observed in **Fig. 8**: *a*) the temperature at 40 cm distance from the PVC pipe was higher than that at 10 cm distance; *b*) the temperature of the upper soil layer was higher than that of the middle soil layer; *c*) the maximum temperature was the same under similar conditions (such as the same site and initial water content), but the maximum temperature was relatively small at Zone C, indicating that a high water content hindered CO_2 migration and carbonation to a great degree; and *d*) the higher the CO_2 ventilation pressure was, the faster the temperature rose, showing that the high ventilation pressure could accelerate the CO_2 migration. The relatively low temperature near the PVC pipe was mainly owing to the absorption of large amounts of heat during the releasing process of compressed CO_2 from the high-pressure tank. Moreover, both CO_2 gas and heat had an upward migration trend, resulting in the higher temperature of the upper soil layer compared to the middle layer.

$$MgO\ (s) + H_2O\ (l) \rightarrow Mg(OH)_2\ (s) \qquad \Delta H=-81\ kJ/mol \tag{5}$$

$$Mg(OH)_2\ (s) + CO_2\ (g) \rightarrow MgCO_3\ (s) + H_2O\ (l) \qquad \Delta H=-37\ kJ/mol \tag{6}$$

Dynamic resilient modulus

330 **Figure 9** shows the dynamic resilient moduli of treated soil layers in different zones
331 before and after carbonation. It can be seen from **Fig. 9** that the average values of dynamic
332 resilient moduli ranged from 4.0 to 10 MPa for MgO-treated soil layers before carbonation,
333 while the moduli significantly increased to 10-25 MPa after 4.5-6 hours' carbonation. Besides,
334 the moduli after carbonation were about three times higher than those before carbonation, and
335 the moduli of four zones had a decreasing trend of A>B>C>D. The moduli of
336 MgO-carbonated soil layers had relatively higher standard deviations compared to
337 MgO-admixed soils, indicating that there was relatively low carbonation homogeneity to
338 some degree. As described by the site conditions, muddy soil layers were too weak (shear
339 strength < 5 kPa) to be tested for the dynamic modulus and dynamic cone penetrometer
340 before treatment, even though the water content was reduced to the liquid limit. Among the
341 reasons for the above results, the hydration of MgO facilitated the further reduction in the
342 water content of muddy soils, and the hydration product formed could generate some
343 cementation under proper compaction effect. In addition, the carbonation products formed
344 after carbonation would generate stronger cementation and compactness, leading to a
345 significant growth of the dynamic resilient modulus which was affected by the initial water
346 content.

347 **Dynamic cone penetrometer test**

348 **Figure 10** presents the variations in blow counts of dynamic cone penetrometer with the
349 penetration depth. Since the average thickness of mud in the ditch pond was about 1.0 m, the
350 subsequent calculation of DCPI was only in accordance with the thinnest depth (~60 cm). As
351 shown in **Fig. 10**, the blow counts increased with the penetration depth, and the increment rate

after carbonation was significantly larger than that before carbonation. **Figure 11** shows the variations in DCPI of treated soil layers in different zones. It can be seen from **Fig. 11** that the DCPI values ranged from 2.5 to 5 mm/blow for treated soil layers before carbonation, while they decreased to 1.0-2.0 mm/blow after several hours' carbonation. These results were consistent with the variations in temperatures and dynamic resilient moduli reported in the above section.

In addition to DCPI, the soil resistance was also obtained from dynamic cone penetrometer tests to evaluate the strength and bearing capacity of treated muddy soil layers. **Figure 12** shows the variations in soil resistance with the penetration depth in four zones. It can be observed from **Fig.12 (a)** that there were some variations in soil resistance among the four zones. The soil resistance along the penetration depth was greatly impacted by the CO_2 carbonation. The soil resistance of MgO-treated soil layers after carbonation (30-40 J/cm) was obviously higher than that before carbonation (< 20 J/cm), and the soil resistances along the penetration depth were identical for most of testing points in the same zones. The discrepancies in soil resistances of different zones principally resulted from the different initial water contents and carbonation conditions. The average values of soil resistances were provided to address the effects of initial water contents and carbonation conditions on soil resistances. It can be seen that owing to the high initial water content and slight compaction, the average values of soil resistances in zones A and B were larger than those in zones C and D.

Direct shear test

Direct shear tests were implemented on raw soils and carbonated/uncarbonated

MgO-admixed soil samples in different zones. **Table 4** shows the fitting relationship between the shear strength and normal stress, as well as shear strength parameters (internal friction angle and cohesion) for different soils. According to **Table 4**, it can be observed that the internal friction angle and cohesion for MgO-admixed soils were slightly higher than those of raw soils, which may be attributed to the effects of hydration products. After carbonation, the internal friction angle and cohesion had significant increments compared to raw soils and MgO-admixed soils. The reason for this result was that the hydration and carbonation products yielded very large internal friction angles and high cohesion due to various angular particle shapes and rough surfaces. The increase in dry density together with the interlocking between particles resulted in significant increments in the internal friction angle and the resistance to shear deformation. Furthermore, these differences for four zones might result from the uniformity of tested samples.

Physical and chemical properties

Table 5 shows the comparisons of physical properties including water content, specific gravity, Atterberg limits and pH value for raw soils, MgO-admixed soils and MgO-carbonated soils. It can be found from **Table 5** that the water content, specific gravity, liquid limit, plasticity index, LOI value and clay particle content of raw soils had significant reductions while both pH value and sandy particle content had considerable increments after admixing with MgO. Similarly, the corresponding physical indexes and pH values continued to drop for MgO-admixed soils in different zones when subjected to carbonation. The above results were basically consistent with previous laboratory studies (Liu et al. 2020). These findings were ascribed to the following reasons: *a*) the alkaline oxide of MgO consumed large amounts of

water through the hydration reaction, facilitating the granulation of soft soils, and resulting in the reduction of water content, specific gravity, liquid limit and plasticity index, as well as the increase of the pH values; *b*) under the CO_2 ventilation and carbonation, the water vapor was expelled by the gaseous CO_2, and the MgO-stabilized soils tended to generate hydrated magnesium carbonates, leading to the agglomeration of soil particles and the continual reduction of water content, liquid limit and plasticity index; and *c*) some OH^- ions were consumed during the CO_2 carbonation, causing a significant reduction of pH values (Cai et al. 2015). The change scopes of physical and chemical indexes in zones A and B were much larger than those in zones C and D, which were mainly caused by the difference of their initial water content. Moreover, the combination with high initial water content and fine-particle soil greatly influenced the migration and infiltration of CO_2, weakening the carbonation degree for zones C and D to some degree (Cai et al. 2015, 2020; Liu et al. 2020). As a result, the incomplete carbonation would further yield a relatively small change in water content, specific gravity, liquid limit, plasticity index, pH value as well as silt and sandy contents compared to MgO-admixed soils.

Mechanism analysis

Figure 14 exhibits the X-ray diffractogram of raw soils as well as uncarbonated and carbonated MgO-admixed soils in zones A and C. To scrutinize the evolution of main products, the intensity of XRD results was set on the semi-logarithmic scale. Evidently, there were some strong peaks of quartz at two theta of 26.59° (3.35 Å), 20.83° (4.26 Å) and 50.05° (1.82 Å) in all samples, indicating that quartz was still the main component of soils in spite of admixing with MgO. A weak MgO peak at two theta of 42.87° (2.11 Å) was detected in the

418 tested samples, showing the existence of little unhydrated MgO. The peaks of brucite were
419 also detected at two theta of 38.04° (3.63 Å), 18.60° (4.76 Å) and 19.86° (4.73 Å) in other
420 tested samples except for raw soils. The peak intensities of brucite in carbonated
421 MgO-admixed soils were obviously lower than those in uncarbonated MgO-admixed soils,
422 and the peak intensities in zone C were higher than those in zone A, revealing the relatively
423 less brucite and consequent higher carbonation degree in zone A. Furthermore, there were
424 newly detected peaks of nesquehonite and dypingite/hydromagnesite in carbonated
425 MgO-admixed soils of zones A and C, and these hydrated magnesium carbonates were
426 consistent with those detected in MgO-carbonated soils of previous studies (Cai et al. 2015;
427 Yi et al. 2013*a*, 2013*b*; Liu et al. 2020). It was difficult to distinguish some specific
428 carbonation products of dypingite and hydromagnesite through XRD analyses due to some
429 overlap peaks.

430 **Figure 15** shows the morphology-structure changes of raw soil, MgO-admixed soils and
431 carbonated MgO-admixed soils occurring in four zones based on SEM analyses. There were
432 big pores or distinct boundaries in the micro structure of parent soil, and no binding was
433 observed between clay soil particles (see **Fig. 15(a)**). After admixing MgO with raw soil, the
434 large pores between soil particles were gradually filled to form small pores some of which
435 might even disappear. It could also be detected from high-magnification micrograph that the
436 clay particles were coated and slightly bonded by the flocculation blobs of brucite (see **Fig.**
437 **15(b)**). This finding also explained why the mechanical strength had not significantly
438 improved for uncarbonated MgO-admixed soils (Yi et al. 2013*a*; Cai et al. 2015; Liu et al.
439 2020). When CO_2 gas was transferred into the MgO-admixed soil layers, abundant

440 magnesium carbonates such as elongated prismatic nesquehonite and rosette-like
441 dypingite/hydromagesite were observed in **Figs. 15(c–f)**. Specifically speaking, the prismatic
442 nesquehonite was mainly found in MgO-carbonated soils in the upper layer of zone A, and the
443 clay particles were almost coated and strongly bonded by dense crystals **(Fig. 15(c))**. And in
444 other zones, the massive crystals of dypingite/hydromagesite were found in carbonated
445 MgO-admixed soils and they were mainly responsible for filling of pores and coating of clay
446 particles (**Figs. 15(d–f)**). However, the SEM images from **Figs. 15(c–f)** displayed that the
447 microstructural characteristics of carbonated soils in the upper layers were quite different
448 from those in the lower layers. The amounts of carbonation products in the upper layers were
449 more than those in the lower layers, and the flocculation blobs of brucite were mainly shown
450 in the bottom layers, indicating the less efficiency of ventilation and carbonation in the
451 bottom layers. In addition, the bonding effects of hydration and carbonation products were
452 very weak for the bottom layers, which explained why the strength in the bottom layer was
453 relatively low.

454 **Figure 16** shows the typical EDS results of raw soil, MgO-admixed soil and carbonated
455 MgO-admixed soils. As shown in **Fig. 16(a)**, the native soil had a discontinuous porous
456 structure with visible voids and its essential components should be aluminum oxide and
457 silicon dioxide according to high elemental content of oxygen, aluminum, silicon and carbon.
458 **Figure 16** also demonstrates three different morphologies of flocculation blobs of brucite,
459 prismatic nesquehonite and rosette-like dypingite/hydromagesite, respectively. The EDS
460 elemental analyses of three locations in **Figs. 16(a, b, c)** revealed the presence of Si, Mg, O,
461 Al, C and Ca elements in the carbonated soils, suggesting the variations of (Mg+Ca)/O and

462 (Si+Al)/O ratios. Obviously, the (Si+Al)/O ratios of carbonated MgO-admixed soils
463 decreased while the (Mg+Ca)/O ratios increased compared to uncarbonated MgO-admixed
464 soils. These microstructural results were accountable for the changes of physical, chemical
465 and mechanical properties of the raw, MgO-admixed and MgO-carbonated soils.

466 ## Discussion

467 Previous laboratory studies mainly revealed the improvement mechanism of carbonated
468 MgO-stabilized soils and analyzed the influence of different initial conditions on the physical,
469 mechanical and microstructural properties of treated soils. Concretely speaking, the strength
470 of carbonated MgO-treated soils decreased with the increase in the liquid limit or initial water
471 content of soils, and the reasonably long-time and high-pressure carbonation could
472 significantly facilitate the strength improvement (Yi. et al. 2013*a*, 2013*b*; Cai et al. 2015,
473 2019*a*, 2019*b*; Liu et al. 2020). The results of the present field study were basically consistent
474 with those of previous researches in terms of the influencing laws of initial conditions. What
475 was different was that the field study tried to apply this MgO carbonation technology to the
476 engineering practice of soft soil treatment.

477 The mass carbonation technology of MgO included the successive processes, *viz.*, the
478 homogeneous mixing of MgO powders, gaseous CO_2 injection and subsequent carbonization
479 under a sealed environment. The field studies demonstrated good feasibility of the MgO mass
480 carbonation technique in improving soft soil layers. Different from an Allu agitator, the
481 mixing machine used in this study mainly included a large-diameter double-shaft mixer head
482 which could mix soft soils evenly and efficiently, avoiding the agglomeration of ultra-soft
483 soils in shallow foundations. After even mixing and slight compaction of MgO-admixed soils,

484 the perforated pipes were inserted into the compacted shallow ground, and the CO_2 ventilation
485 was achieved through the method of intubation and injection under the sealing condition.
486 Subsequently, the dynamic cone penetrometer and dynamic deformation modulus were
487 measured respectively. The dynamic cone penetrometer test clearly reflected the physical and
488 mechanical properties of different-depth soil layers and quantitatively determined the
489 compaction degree of these soil layers through observing the variations in penetration
490 resistance with depth. Moreover, different types of deflectometers classified according to load
491 characteristics and number of deflection sensors were commonly available around the world
492 but were very similar in principle. The LWD was a portable device with a small load (10 kN)
493 and a small number of deflection sensors (1−3) compared to falling weight deflectometer with
494 a load of 7−150 kN and 1−18 deflection sensors (Beaulieu et al. 2014). The dynamic
495 deformation modulus measured by LWD was an effective index to reflect the overall bearing
496 capacity of stabilized-soil foundation. There were remarkable variations in penetration
497 resistance with depth in these four zones, indicating that the improvement was not uniform at
498 different depths owing to the high initial water content as well as inhomogeneous ventilation
499 and carbonation of CO_2. However, from the view of dynamic deformation modulus, the
500 foundation of carbonated MgO-admixed soils had a better mechanical strength and structural
501 integrity compared to uncarbonated MgO-admixed soils.

502 Based on the results of mechanical and microstructural characteristics, the improvement
503 mechanism of MgO mass carbonation can be concluded as follows: (*i*) when admixed into
504 wet soils, MgO powders were easily adsorbed on the surface of soil particles under the effect
505 of water films; (*ii*) MgO powders would have hydration reactions with pore water to form

506 expansive brucite (Eq. (5)), reducing the water content of soft soils; (*iii*) similar to
507 lime-stabilized soils, the magnesium ions (i.e., Mg^{2+}) from the hydrolysis of brucite would
508 have the cation-exchange reactions with other cations of clay particles (i.e., Na^{+}, K^{+}),
509 resulting in a substantial reduction in the thickness of diffuse double layers as well as the
510 formation of coarser flocculation blobs between clay particles (Thyagaraj and Zodinsanga
511 2015); and (*iv*) when the CO_2 gas was injected and diffused into MgO-admixed soft soils, a
512 series of hydrated magnesium carbonates were formed through carbonation reactions (Eqs. (7)
513 and (8)). In addition, the dissolved silica and alumina from clay lattices might slowly have the
514 similar pozzolanic reactions with magnesium available in the high alkaline soil. The
515 cementitious compounds such as hydrated magnesium silicate and hydrated magnesium
516 aluminate could also increase the strength of soft soils (Fasihnikoutalab et al. 2017). However,
517 these products from the pozzolanic reactions were not clearly detected in this study owing to
518 the shorter curing time and lower alkalinity. Therefore, the synergistic effects of MgO and
519 CO_2 facilitated the binding of soil particles and filling of pores, and the corresponding
520 carbonates and denser microstructure were the major contributors to the significant and rapid
521 improvement in the mechanical performance of soft-soil subgrades.

522 $$Mg(OH)_2 + CO_2 + H_2O \rightarrow MgCO_3 \cdot 3H_2O \quad (7)$$

523 $$Mg(OH)_2 + CO_2 + H_2O \rightarrow Mg_5(CO_3)_4(OH)_2 \cdot (3 \text{ or } 4)H_2O \quad (8)$$

524 As to the chemically stabilized methods mentioned in the "**Introduction"** section, their
525 stabilization mechanisms varied with curing agents including PC, lime, geopolymers, MgO
526 and so forth. Unlike the carbonation of MgO, the stabilization of PC and lime was achieved
527 through the slow hydration and pozzolanic reactions, and the stabilization of geopolymers

528 was realized through the slow recombination of silicon-oxygen and aluminum-oxygen bonds
529 under the alkali-activated action. According to the stabilization mechanism, various
530 geopolymers in existing studies were made based on the feasibility of industrial wastes
531 including fly ash, slag, carbide slag and metakaolin to a large extent (Mozumder and Laskar
532 2015). Compared to the treatment efficacy and environmental benefits of these binders, the
533 MgO carbonation had significant advantages in the improvement of weak soils such as rapid
534 development of strength (several hours) and potential environmental benefits (CO_2 absorption
535 of 0.88-1.1 times MgO). Besides, the treatment efficiency of MgO-admixed soils was affected
536 by such conditions as MgO activity, initial water content, permeability and CO_2 pressure.
537 Previous laboratory studies revealed that the cost of MgO was close to that of PC for reaching
538 the same strength of stabilized soils in spite that the price of MgO would greatly increase with
539 its activity (Yi et al. 2016; Cai et al. 2019*a*). In this field trial, the cost of MgO with high
540 impurity and low activity was slightly lower than that of PC, and the cost of high-purity CO_2
541 purchased was about half of MgO, leading to the slightly higher project cost of the MgO mass
542 carbonation compared to conventional PC stabilization. Therefore, the overall cost for MgO
543 carbonation would be similar to (or slightly lower than) that of PC stabilization if waste CO_2
544 captured from industries or atmosphere could be used for free in carbonation.

545 The field tests as the first attempt encountered some construction difficulties and
546 application limitations though relatively satisfying mechanical properties could be gained for
547 the soft soil foundation after the MgO mass carbonation treatment. These difficulties and
548 limitations mainly included: (*i*) there was occasional powder blockage due to a small amount
549 of MgO caking caused by long-time stacking and humid environment outside the feed tank

(Fig. 2(a) and Fig. 3(b)); (*ii*) when the thickness of the soft soil layer was less than 1.0 m, there was obvious powder leakage and waste of MgO during the mixing process (Fig. 5(a)); (*iii*) the CO_2 discharged from high-pressure tanks easily caused the pipes to freeze; and (*iv*) the CO_2 gas migration and diffusion as well as subsequent carbonation were still uneven from the top to the bottom of soil layers through intubation, owing to the moist-vapor redistribution and the unevenness of compaction degree. Moreover, the present field study was limited to the muddy soil with high water content, high liquid limit as well as low permeability, which made the abovementioned shortages more prominent. Consequently, it is necessary to elaborately refine the construction equipment and operation conditions for the real-life applications of MgO mass carbonation in soft-soil fields. Future endeavors should be made in the following aspects: (*i*) a fine sieve should be placed onto the feed tank to filter out the fragments or particles of MgO, and the powder spraying mouth needs to be improved to avoid the dust leakage of MgO; (*ii*) the CO_2 pipes should be kept through the electric heater to prevent the pipes from freezing; (*iii*) this mass carbonation technique might be more suitable for soils with low water content, low liquid limit, large void ratio (e.g., silty and sandy soils) under a non-freezing environment; (*iv*) the in-situ ectopic mixing method can also be used in the mixing of shallow soft soils; and (*v*) the collection of waste CO_2 needs to be studied to further save the project cost. Overall, the outcomes of this field investigation will contribute to the utilization of the combined stabilizer of MgO and CO_2 and the mass carbonation technology in subgrade improvement.

Conclusions

This study presents a field investigation of the shallow soft-soil highway subgrade

572 treated by the mass carbonation technology. The MgO and CO_2 were used as the combined
573 curing binders, and the physical and mechanical properties of the soft ground before and after
574 carbonation were compared in four different zones. Based on the research results, the main
575 findings can be summarized as follows:

576 (1) During the CO_2 ventilation periods, the temperature of the MgO-stabilized soil, far
577 higher than the average ambient temperature, firstly increased to reach the maxima before 3
578 hours and then began to decrease after remaining stable temporarily.

579 (2) The average values of dynamic resilient moduli were 4.0-10 MPa for treated soil
580 layers before carbonation, while the moduli had a great increase and reached 10-25 MPa after
581 carbonation of 4.5-6 hours. The moduli after carbonation were about three times higher than
582 those before carbonation, and the moduli of several zones had a decreasing trend of
583 A>B>C>D.

584 (3) DCPI values ranged from 2.5-5 mm/blow and 1.0-2.0 mm/blow for MgO-admixed
585 soil layers before and after carbonation, respectively. The soil resistance of treated soil layers
586 after carbonation (30-40 J/cm) was obviously higher than that before carbonation (< 20 J/cm),
587 and the soil resistance along penetration depth was identical for most of the testing points at
588 the same zones.

589 (4) The friction angle and cohesion of MgO-admixed soils slightly increased compared
590 to the raw soil while the two parameters had a significant increase after carbonation. Besides,
591 the water content, specific gravity, liquid limit, plasticity index, LOI value and clay particle
592 content of the raw soil had some decrease while both the pH value and sandy particle content
593 had a great increase after admixing with the MgO powder. The above physical indexes as well

as pH values continued to drop significantly in different zones after CO_2 carbonation, and the changed scopes of physical and chemical indexes in zones A and B were much larger than those in zones C and D.

(5) The stabilization mechanism of the MgO mass carbonation was discussed through XRD, SEM and EDS analyses. The improvement of engineering properties could be attributed to the cementation effects of hydrated carbonates and filling of pores. It is beneficial for further understanding the potential of the MgO mass carbonation technology in soft ground reinforcement.

Acknowledgements

The authors would like to thank Chuan Qin and Ye Ye at Southeast University, and Nenghe Gong and Yiming Ding at Nanjing Luding Stirring Pile Special Technology Co. Ltd., and Guanzhong Bo et al. at China Communication Bureau for their assistance in field tests.

The authors also greatly appreciate the funding provided by the NSFC (41902286, 41972269, 41977241), the Natural Science Foundation of the Jiangsu Higher Education Institutions of China (18KJB560012), the Youth Science and Technology Innovation Fund of Nanjing Forestry University (CX2018005), Science and Technology Project of Jiangsu Traffic Engineering Construction Bureau (2018T01), Open Fund for State Key Laboratory of Geotechnical Mechanics and Engineering (Z019026), and Ministry of Housing and Urban-rural Development Science and Technology Project Plan (2018-K7-013).

References

Abdullah, H.H., Shahin, M.A., Walske, M.L., and Karrech, A. 2020. Systematic approach to

assessing the applicability of fly-ash based geopolymer for clay stabilization. Canadian Geotechnical Journal, doi: 10.1139/cgj-2019-0215.

Abiodun, A.A., and Nalbantoglu, Z. 2015. Lime pile techniques for the improvement of clay soils. Canadian Geotechnical Journal, 52: 760–768. doi: 10.1139/cgj-2014-0073.

Acar, Y.B. Puppala, A.J., Seals, R.K. 1991. Calibration of a dynamic penetrometer for compaction quality control of boiler slag. Geotechnical Testing Journal, 14(1), 56-63. doi: 10.1520/GTJ10191J.

Arulrajah, A., Piratheepan, J., Bo, M.W., and Sivakugan, N. 2012. Geotechnical characteristics of recycled crushed brick blends for pavement sub-base applications. Canadian Geotechnical Journal, 49(7): 796–811. doi: 10.1139/t2012-041.

Arulrajah, A., Mohammadinia, A., Phummiphan, I., Horpibulsuk, S., and Samingthong, W. 2016. Stabilization of recycled demolition aggregates by geopolymers comprising calcium carbide residue, fly ash and slag precursors. Construction and Building Materials, 114, 864–873. doi: 10.1016/j.conbuildmat.2016.03.150.

ASTM. 2007*a*. Standard test method for particle-size analysis of soils. ASTM standard D422. ASTM International, West Conshohocken, Pa. doi:10.1520/D0422-63R07E02.

ASTM. 2007*b*. Standard test method for pH of soils. ASTM standard D4972. ASTM International, West Conshohocken, Pa. doi: 10.1520/D4972-01R07.

ASTM. 2009. Standard test method for use of the dynamic cone penetrometer in shallow pavement applications. ASTM standard D6951 M-09. ASTM International, West Conshohocken, Pa.

ASTM. 2010*a*. Standard test methods for liquid limit, plastic limit and plasticity index of

638 soils. ASTM standard D4318. ASTM International, West Conshohocken, Pa. doi:
639 10.1520/D4318-10.
640 ASTM. 2010*b*. Standard methods for specific gravity of soils by water pycnometer. ASTM
641 standard D854. ASTM International, West Conshohocken, Pa. doi: 10.1520/D0854-10.
642 ASTM. 2011*a*. Standard practice for classification of soils for engineering purposes (Unified
643 Soil Classification System). ASTM standard D2487. ASTM International, West
644 Conshohocken, Pa. doi: 10.1520/D2487-11.
645 ASTM. 2011*b*. Standard test method for direct shear test of soils under consolidated drained
646 conditions. ASTM standard D3080M-11. ASTM International, West Conshohocken, Pa.
647 doi: 10.1520/D3080-D3080M-11.
648 ASTM. 2011*c*. Standard test method for measuring deflections with a light weight
649 deflectometer (LWD). ASTM standard E2583-07R11. ASTM International, West
650 Conshohocken, Pa. doi: 10.1520/E2583-07R11.
651 ASTM. 2016. Standard test method for mechanical cone penetration tests of soil. ASTM
652 standard D3441-16. ASTM International, West Conshohocken, Pa. doi:
653 10.1520/D3441-16.
654 Bo, M. W., Arulrajah, A., Horpibulsuk, S., and Leong, M. 2015. Quality management of
655 prefabricated vertical drain materials inmega land reclamation projects: A case study.
656 Soils and Foundations, 55(4), 895–905. doi: 10.1016/j.sandf.2015.06.019.
657 Beaulieu, L., Pleau, R., Pierre, P., Poulin, P., and Juneau, S. Mechanical performance in field
658 conditions of treated and stabilized granular materials used in unpaved roads: a
659 longitudinal study. Canadian Journal of Civil Engineering, 2014, 41(2): 97-105.

660 10.1139/cjce-2012-0423.

661 Burnham, T.R. 1997. Application of the dynamic cone penetrometer to Minnesonta
662 Department of Transportation, pavement assessment procedures. Minnesota Department
663 of Transportation, Maplewood, MN, USA, MN/RC-97/19.

664 Cai, G.H., Du, Y.J., Liu, S.Y., and Singh, D.N. 2015. Physical properties, electrical resistivity
665 and strength characteristics of carbonated silty soil admixed with reactive magnesia.
666 Canadian Geotechnical Journal, 52(11): 1699–1713. doi: 10.1139/cgj-2015-0053.

667 Cai, G.H., Liu, S.Y., and Zheng, X. 2019*a*. Effects of drying-wetting cycles on the durability
668 of carbonated reactive magnesia-admixed clayey soil. Journal of Materials in Civil
669 Engineering, 31(11): 04019276(1-13). doi: 10.1061/(ASCE)MT.1943-5533.0002940.

670 Cai, G.H., Liu, S.Y., Du, G.Y., and Wang, L. 2019*b*. Effect of MgO activity index on
671 physicochemical and electrical properties of carbonated silt. KSCE Journal of Civil
672 Engineering, 23(9): 3807-3817. doi: 10.1007/s12205-019-0955-8.

673 Cai, G.H., Liu, S.Y., Du, G.Y., Wang, L., Li, J.S., and Liu, L. 2020. Hydraulic conductivity
674 characteristics of carbonated reactive magniesia-treated silt. Bulletin of Engineering
675 Geology and the Environment, 23(9): 3807-3817. doi: 10.1007/s10064-020-01746-6.

676 Cai, Y.Q., Xie, Z.W., Wang, J., Wang, P., and Geng, X.Y. 2018. New approach of vacuum
677 preloading with booster prefabricated vertical drains (PVDs) to improve deep marine
678 clay strata. Canadian Geotechnical Journal, 55: 1359–1371. doi: 10.1139/cgj-2017-0412.

679 Chai, J., Horpibulsuk, S., Shen, S.L., and Carter, J.P. 2014. Consolidation analysis of clayey
680 deposits under vacuum pressure with horizontal drains. Geotextiles and Geomembranes,
681 42(5): 437-444. doi: 10.1016/j.geotexmem.2014.07.001.

682 Chakrabarti, S., and Kodikara, J.K. 2007. Direct tensile failure of cementitiously stabilized
683 crushed rock materials. Canadian Geotechnical Journal, 44(2): 231–240. doi:
684 10.1139/t06-102.
685 Chian, S.C., Nguyen, S.T., and Phoon, K.K.. 2016. Extended strength development model of
686 cement-treated clay. Journal of Geotechnical and Geoenvironmental Engineering, 142(2):
687 06015014. doi: 10.1061/(ASCE)GT.1943-5606.0001400.
688 China NRA. 2018. Code for in-situ testing of railway engineering geology. National Railway
689 Administration of China, Beijing, China, TB 10018–2018.
690 China JTG. 2008. Field Test Methods of subgrade and pavement for highway engineering.
691 Ministry of Transportation of China, Beijing, China, E60-2008.
692 Diniz, D.H., Carvalho J.M.F., Mendes J.C. and Peixoto R.A.F. 2017. Blast oxygen furnace
693 slag as chemical soil stabilizer for use in roads. Journal of Materials in Civil
694 Engineering, 2017, 29(9): 04017118(1-7). doi: 10.1061/(ASCE)MT.1943-5533.0001969.
695 Du, Y.J., Jiang, N.J., Liu, S.Y., Horpibulsuk, S., Arulrajah, A. 2016. Field evaluation of soft
696 highway subgrade soil stabilized with calcium carbide residue. Soils and Foundations,
697 56(2):301-314. doi: 10.1016/j.sandf.2016.02.012.
698 Fang, Y.S., Chung, Y.T., Yu, F. J., and Chen, T.J. 2001. Properties of soil-cement stabilized
699 with deep mixing method. Ground Improvement, 5(2): 69-74. doi:
700 10.1680/grim.2001.5.2.69.
701 Fasihnikoutalab, M.H., Asadi, A., Unluer, C., Huat, B.K., Ball, R.J., and Pourakbar, S. 2017.
702 Utilization of alkali-activated olivine in soil stabilization and the effect of carbonation on
703 unconfined compressive strength and microstructure. Journal of Materials in Civil

704 Engineering, 29(6): 06017002(1-11). doi: 10.1061/(ASCE)MT.1943-5533.0001833.
705 Han, J., Oztoprak, S., Parsons, R.L., and Huang, J. 2007. Numerical analysis of foundation
706 columns to support widening of embankments. Computers and Geotechnics, 34(6):
707 435–448. doi:10.1016/j.compgeo.2007.01.006.
708 Horpibulsuk, S., Phetchuay, C., and Chinkulkijniwat, A. 2012. Soil stabilization by calcium
709 carbide residue and fly ash. Journal of Materials in Civil Engineering, 24(2): 184–193.
710 doi: 10.1061/(ASCE)MT.1943-5533.0000370.
711 Horpibulsuk, S., Phetchuay, C., Chinkulkijniwat, A., and Cholaphatsorn, A. 2013. Strength
712 development in silty clay stabilized with calcium carbide residue and fly ash. Soils and
713 Foundation, 53(4): 477–486. doi: 10.1016/j.sandf.2013.06.001.
714 Hoang, T., Alleman, J., Cetin, B., Ikuma, K., and Choi, S.G. 2019. Sand and silty-sand soil
715 stabilization using bacterial enzyme–induced calcite precipitation (BEICP). Canadian
716 Geotechnical Journal, 56: 808–822. doi: 10.1139/cgj-2018-0191.
717 Howayek, A.E., Bobet, E., and Santagata, M. 2019. Microstructure and cementation of two
718 carbonatic fine-grained soils. Canadian Geotechnical Journal 56: 320–334. doi:
719 10.1139/cgj-2018-0059.
720 Jelistic, N., and Leppanen, M. 2003. Mass stabilization of organic soils and soft clay. Third
721 International Conference on Grouting and Ground Treatment, Grouting 2003, 552-561.
722 doi: 10.1061/40663(2003)28.
723 Jiang, N.J., Du, Y.J., Liu, S.Y., Wei, M.L., Horpibulsuk, Suksun., and Arulrajah, A. 2016.
724 Multi-scale laboratory evaluation of the physical, mechanical, and microstructural
725 properties of soft highway subgrade soil stabilized with calcium carbide residue.

726 Canadian Geotechnical Journal, 53: 373–383. doi: 10.1139/cgj-2015-0245.
727 Kampala, A., Horpibulsuk, S., Chinkullijniwat, A., and Shen, S.L. 2013. Engineering
728 properties of recycled calcium carbide residue stabilized clay as fill and pavement
729 materials. Construction and Building Materials, 46: 203–210. doi:
730 10.1016/j.conbuildmat.2013.04.037.
731 Latifi, N., Vahedifard, F., Ghazanfari, E., and Eashid, A.S.A. 2018. Sustainable usage of
732 calcium carbide residue for stabilization of clays. Journal of Materials in Civil
733 Engineering, 30(6): 04018099(1-10). doi: 10.1061/(ASCE)MT.1943-5533.0002313.
734 Liska, M., Vandeperre, L.J., and Al-Tabbaa, A. 2008. Influence of carbonation on the
735 properties of reactive magnesia cement-based pressed masonry units. Advances in
736 Cement Research, 20(2): 53–64. doi: 10.1680/adcr.2008.20.2.53.
737 Liu, P., Shao, G.H., and Huang, R.P. 2019. Study of the interactions between S. pasteurii and
738 indigenous bacteria and the effect of these interactions on the MICP. Arabian Journal of
739 Geosciences, 12(23): 724(1-10). doi: 10.1007/s12517-019-4840-z.
740 Liu, S.Y., Du, Y.J., Yi, Y.L., and Puppala, A.J. 2012. Field investigations on performance of
741 T-shaped deep mixed soil cement column–supported embankments over soft ground.
742 Journal of Geotechnical and Geoenvironmental Engineering, 138: 718–727. doi:
743 10.1061/(ASCE)GT.1943-5606.0000625.
744 Liu, S.Y., Cai, G.H., Cao, J.J., and Wang, F. 2020. Influence of soil type on strength and
745 microstructure of carbonated reactive magnesiatreated soil. European Journal of
746 Environmental and Civil Engineering, 24(2): 248-266. doi:
747 10.1080/19648189.2017.1378925.

748 Lu, W.H., Miao, L.C., Wang, F., Zhang, J.H., Zhang, Y.X., and Wang, H.B. 2019. A case
749 study on geogrid-reinforced and pile-supported widened highway embankment.
750 Geosynthetics International, doi: 10.1680/jgein.19.00024.
751 Madhyannapu, R.S., Puppala, A.J., Nazarian, S., and Yuan, D. 2010. Quality assessment and
752 quality control of deep soil mixing construction for stabilizing expansive subsoils.
753 Journal of Geotechnical and Geoenvironmental Engineering, 136(1): 119-128. doi:
754 10.1061/ASCEGT.1943-5606.0000188.
755 Martin, J.T., Bryan, A.M., and Alan, L.B. 2012. Experiences of dry soil mixing in highly
756 organic soils. Ground Improvement, 165(GI1): 3-14. doi: 10.1680/grim.2012.165.1.3.
757 Martin, J.T., and Bryan, A.M. 2017. Strength verification of stabilized soil–cement columns:
758 a laboratory investigation of the push-in resistance test (PIRT). Canadian Geotechnical
759 Journal, 54(6): 789–805. doi: 10.1139/cgj-2016-0230.
760 Mohammadi, S.D., Nikoudel, M.R., Rahimi, H., and Khamehchiyan, M. 2008. Application of
761 the Dynamic Cone Penetrometer (DCP) for determination of the engineering parameters
762 of sandy soils. Engineering Geology, 101(3-4): 195-203. doi:
763 10.1016/j.enggeo.2008.05.006.
764 Mozumder, R.A., and Laskar, A.I. 2015. Prediction of unconfined compressive strength of
765 geopolymer stabilized clayey soil using Artificial Neural Network. Computers and
766 Geotechnics, 69: 291-300. doi: 10.1016/j.compgeo.2015.05.021.
767 Shen, S.L., Wang, Z., Yang, J., and Ho, C. 2013. Generalized approach for prediction of jet
768 grout column diameter. Journal of Geotechnical and Geoenvironmental Engineering,
769 139(12): 2060–2069. doi:10.1061/(ASCE)GT.1943-5606.0000932.

770 Sukmak, P., Horpibulsuk, S., Shen, S.L., Chindaprasirt, P., and Suksiripattanapong, C. 2013.
771 Factors influencing strength development in clay–fly ash geopolymer. Construction and
772 Building Materials, 47: 1125–1136, doi: 10.1016/j.conbuildmat.2013.05.104.
773 Thyagaraj, T., and Zodinsanga, S. 2015. Laboratory investigations of in situ stabilization of
774 an expansive soil by lime precipitation technique. Journal of Materials in Civil
775 Engineering, 27(7): 06014028(1-8). doi: 10.1061/(ASCE)MT.1943-5533.0001184.
776 Unluer, C., and Al-Tabbaa, A. 2013. Impact of hydrated magnesium carbonate additives on
777 the carbonation of reactive MgO cements. Cement and Concrete Research, 54: 87–97.
778 doi: 10.1016/j.cemconres.2013.08.009.
779 Unluer, C., and Al-Tabbaa, A. 2015. The role of brucite, ground granulated blastfurnace slag,
780 and magnesium silicates in the carbonation and performance of MgO cements.
781 Construction and Building Materials, 94: 629–643. doi:
782 10.1016/j.conbuildmat.2015.07.105.
783 Wang, J., Cai, Y., Ma, J., Chu, J., Fu, H., Wang, P., and Jin, Y.W. 2016. Improved vacuum
784 preloading method for consolidation of dredged clay-slurry fill. Journal of Geotechnical
785 and Geoenvironmental Engineering, 142(11): 06016012. doi:
786 10.1061/(ASCE)GT.1943-5606.0001516.
787 Wang, J., Fu, H., Liu, F., Cai, Y., and Zhou, J. 2018. Influence of electro-osmosis activation
788 time on vacuum electro-osmosis consolidation of a dredged slurry. Canadian
789 Geotechnical Journal, 55(1): 147–153. doi: 10.1139/cgj-2016-0687.
790 Wheeler, L.N., Take, W.A., and Hoult, N.A. 2017. Performance assessment of peat rail
791 subgrade before and after mass stabilization. Canadian Geotechnical Journal, 54(5):

674–689. doi: 10.1139/cgj-2016-0256.

Wilk, C.M. 2014. Stabilization of marginal soil in new and existing right-of-way. In Proceedings of the AREMA2014 Annual Conference & Exposition, Chicago, Ill.

Xia, W.Y., Du, Y.J., Li, F.S., Li, C.P., Yan, X.L., Arulrajah, A., Wang, F., and Song, D.J. 2019. In-situ solidification/stabilization of heavy metals contaminated site soilusing a dry jet mixing method and new hydroxyapatite based binder. Journal of Hazardous Materials 369: 353–361. doi: 10.1016/j.jhazmat.2019.02.031.

Yi, Y., Liaka, M., Unluer, C., and Al-Tabbaa, A. 2013*a*. Carbonating magnesia for soil stabilization. Canadian Geotechnical Journal, 50(8): 899–905, doi: 10.1139/cgj-2012-0364.

Yi, Y., Liska, M., Akinyugha, A., Unluer, C., and Al-Tabbaa, A. 2013*b*. Preliminary laboratory-scale model auger installation and testing of carbonated soil-MgO columns. Geotechnical Testing Journal, 36(3): 384-393. doi: 10.1520/GTJ20120052.

Yi, Y., Gu, L., and Liu, S. 2015*a*. Microstructural and mechanical properties of marine soft clay stabilized by lime-activated ground granulated blastfurnace slag. Applied Clay Science, 103: 71–76. doi:10.1016/j.clay.2014.11.005.

Yi, Y.L., Gu, L.Y., Liu, S.Y., and Puppala, A.J. 2015*b*. Carbide slag–activated ground granulated blastfurnace slag for soft clay stabilization. Canadian Geotechnical Journal, 52: 656–663. doi: 10.1139/cgj-2014-0007.

Yi, Y.L., Lu, K.W., Liu, S.Y., and Al-Tabbaa, A. 2016. Property changes of reactive magnesia-stabilized soil subjected to forced carbonation. Canadian Geotechnical Journal, 53(2): 314–325. doi:10.1139/cgj-2015-0135.

814 Zamani, A., Montoya, B.M., and Mohammed, A.G., 2019. Investigating challenges of in situ
815 delivery of microbial-induced calcium carbonate precipitation (MICP) in fine-grain
816 sands and silty sand. Canadian Geotechnical Journal, 56: 1889–1900. doi:
817 10.1139/cgj-2018-0551.
818 Zhang, Y.X., Fang, Y., Lu, W.H., Liu, C., Wang, L., Xie, H., and Zhang, X.M. 2019.
819 Shrinkage behavior influence of strain hardening cementitious composites. Structural
820 Concrete, 1-9. doi: 10.1002/suco.201800327
821 Zhang, T., Yang, Y.L., and Liu, S.Y. 2020. A shear model for solidified soils considering
822 conservation of energy. Computers and Geotechnics, 120, 103439: 1-13. doi:
823 10.1016/j.compgeo.2020.103439.
824 Zhao, Z.F., Zhou, M., Hu, Y.X., and Hossain, M.S. 2018. Behavior of soil heave inside
825 stiffened caissons being installed in clay. Canadian Geotechnical Journal, 55(5):
826 698-709. doi: 10.1139/cgj-2016-0667.

828 **Table lists**

835

837 **Table 1** Physical and chemical properties of experimental materials.

Property	Index value	
	Mud soil	MgO
Natural water content, w (%)	56~64	
Liquid limit, w_L (%)	46	
Plastic limit, w_P (%)	20	
Plasticity index	26	
Specific gravity, G_s	2.70	2.45
pH (soil: water=1:1) [a]	7.4	
Specific surface area (m^2/g) [b]		7.21
Activity content (%)		62
Grain size distribution (%)[c]		
Clay (< 0.002 mm)	15.6	28.9
Silt (0.002-0.074 mm)	83.3	71.1
Sand (0.074-20 mm)	1.1	0

838 **Note:** [a] Based on ASTM D4972 (ASTM, 2013);

839 [b] Measured using the BET method via a physisorption analyzer;

840 [c] Measured using a laser particle-size analyzer "Mastersizer 2000" (Malvern, USA).

841

Table 2 Chemical compositions of experimental materials.

Oxides contents (%) [a]	Value	
	Mud soil	MgO
Silicon dioxide (SiO_2)	69.79	5.58
Aluminum oxide (Al_2O_3)	17.84	0.42
Iron oxide (Fe_2O_3)	5.34	0.22
Potassium oxide (K_2O)	2.05	0.01
Calcium oxide (CaO)	1.11	2.46
Magnesium oxide (MgO)	1.04	81.33
Titanium oxide (TiO_2)	1.00	ND
Sulfur trioxide (SO_3)	ND [c]	0.1
LOI [b] (%)	4.8	9.88

Note: [a] Measured using an X-ray fluorescence spectrometry (EDXRF);

[b] Value of loss on ignition is referenced to 950°C;

[c] ND, Not detected.

Table 3 Initial water content and ventilation characteristics of all zones.

Zone	Initial water content (%)	Total ventilation pressure (MPa)	Duration time (h)
A	45	1.5	6
B	47	2.5	4.5
C	53	1.5	6
D	56	2.5	4.5

Table 4 Fitting equations and parameters of shear strength for different soils.

Samples	Fitting equations	Internal friction angle, Φ (°)	Cohesion, c (kPa)
Raw soil	τ=0.16σ+14.3 (R^2=0.99)	9.34	14.32
MgO-admixed soil	τ=0.19σ+15.1 (R^2=0.99)	10.65	15.06
MgO-carbonated soil (zone A)	τ=0.35σ+55.0 (R^2=0.94)	19.10	55.03
MgO-carbonated soil (zone B)	τ=0.43σ+47.2 (R^2=0.98)	23.17	47.23
MgO-carbonated soil (zone C)	τ=0.49σ+46.7 (R^2=0.99)	25.98	46.71
MgO-carbonated soil (zone D)	τ=0.37σ+47.9 (R^2=0.99)	20.33	47.92

Table 5 Comparison of physical properties for raw soil, MgO-admixed soil and MgO-carbonated soil.

Property	Raw soil	MgO-admixed soil	Zones of MgO-carbonated soil			
			A	B	C	D
Water content/%	45-47 (Zone A, B) 53-56 (Zone C, D)	34-37(Zone A, B) 42-45 (Zone C, D)	26.8	28.2	34.6	37.4
Specific gravity	2.70	2.69	2.66	2.66	2.68	2.69
Liquid limit, w_L/%	46.4	40.5	34.2	34.8	36.6	37.0
Plastic limit, w_P /%	20.8	20.4	18.4	18.2	17.8	17.6
Plasticity index	25.6	20.1	15.8	16.6	18.8	19.4
LOI/%	4.6	4.2	3.5	3.5	3.8	4.0
pH value	7.42	10.25	9.31	9.42	9.63	9.86
Particle distribution (%)						
Clay (< 0.002 mm)	15.6	6.0	3.5	3.9	4.6	4.8
Silt (0.002-0.074 mm)	83.3	83.5	68.5	71.5	78.9	79.8
Sand (0.074-20 mm)	1.1	10.5	28	24.6	16.5	15.8

Figure lists

Fig. 1 Location and field view of the test site in Yixing of Jiangsu Province, China: (a) the location map from Google Earth; (b) the field scene before treatment.

Fig. 2 In-situ experimental materials: (a) industrial MgO; (b) PE pipe; (c) perforated PVC pipe; (d) quick union; (e) high-pressure pipe; and (f) CO_2 tank.

Fig. 3 Main apparatus of in-situ construction: (a) mixing system; (b) binder spraying system; (c) alternator; (d) air compressor; and (e) assembly drawing of system.

Fig. 4 Flow chart of the construction procedure for the mass carbonation treatment.

Fig. 5 Overview of in-situ construction procedure for mass carbonation treatment: (a) mixing MgO powder; (b) secondary mixing; (c) ditching; (d) inserting PVC; (e) connecting vent pipe; and (f) sealing and carbonating.

Fig. 6 Arrangement diagram of vent pipes: (a) cross-sectional drawing; and (b) plane drawing.

Fig. 7 Layout of field tests: (a) field picture; and (b) diagrammatic figure.

Fig. 8 Variation in temperature of MgO-stabilized soil layers during CO_2 ventilation process.

Fig. 9 Dynamic resilient modulus of treated soil layers at different zones ground before and after carbonation: (a) dynamic resilient modulus; and (b) average dynamic resilient modulus.

Fig. 10 Variations in blow counts of treated soil layers with penetration depth.

Fig. 11 Variations in dynamic cone penetration index (DCPI) of treated soil layer at different zones: (a) DCPI; and (b) average DCPI.

Fig. 12 Variations in the soil resistance of treated soil layers with penetration depth: (a) soil

resistance; and (b) average soil resistance.

Fig. 13 Variations in bearing capacity of treated soil layers at different zones: (a) bearing capacity; and (b) average bearing capacity.

Fig. 14 XRD results of raw soil, MgO-admixed soil and MgO-carbonated soils.

Fig. 15 SEM images of raw soil, MgO-admixed soil and MgO-carbonated soils of different treatment zones: (a) raw soil; (b) MgO-admixed soil; (c) MgO-carbonated soil (zone A); (d) MgO-carbonated soil (zone B); (e) MgO-carbonated soil (zone C); and (f) MgO-carbonated soil (zone D).

Fig. 16 EDS results of raw soil, MgO-admixed soil and MgO-carbonated soils: (a) Raw soil; (b) MgO-admixed soil; (c) MgO-carbonated soil (zone A); and (d) MgO-carbonated soil (zone C) (Note: the upper part indicates electronic images and the lower part indicates EDS results of designated areas).

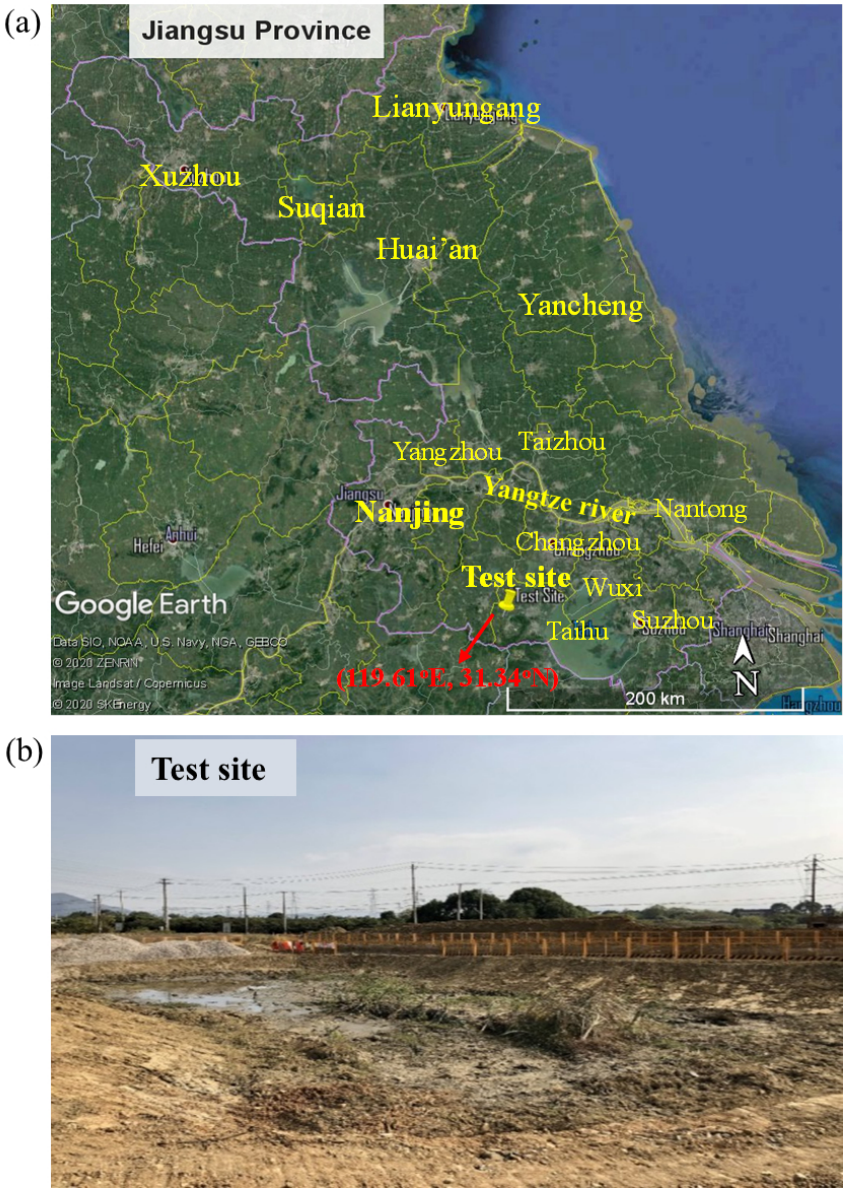

Fig. 1 Location and field view of the test site in Yixing of Jiangsu Province, China: (a) the location map from Google Earth; (b) the field scene before treatment.

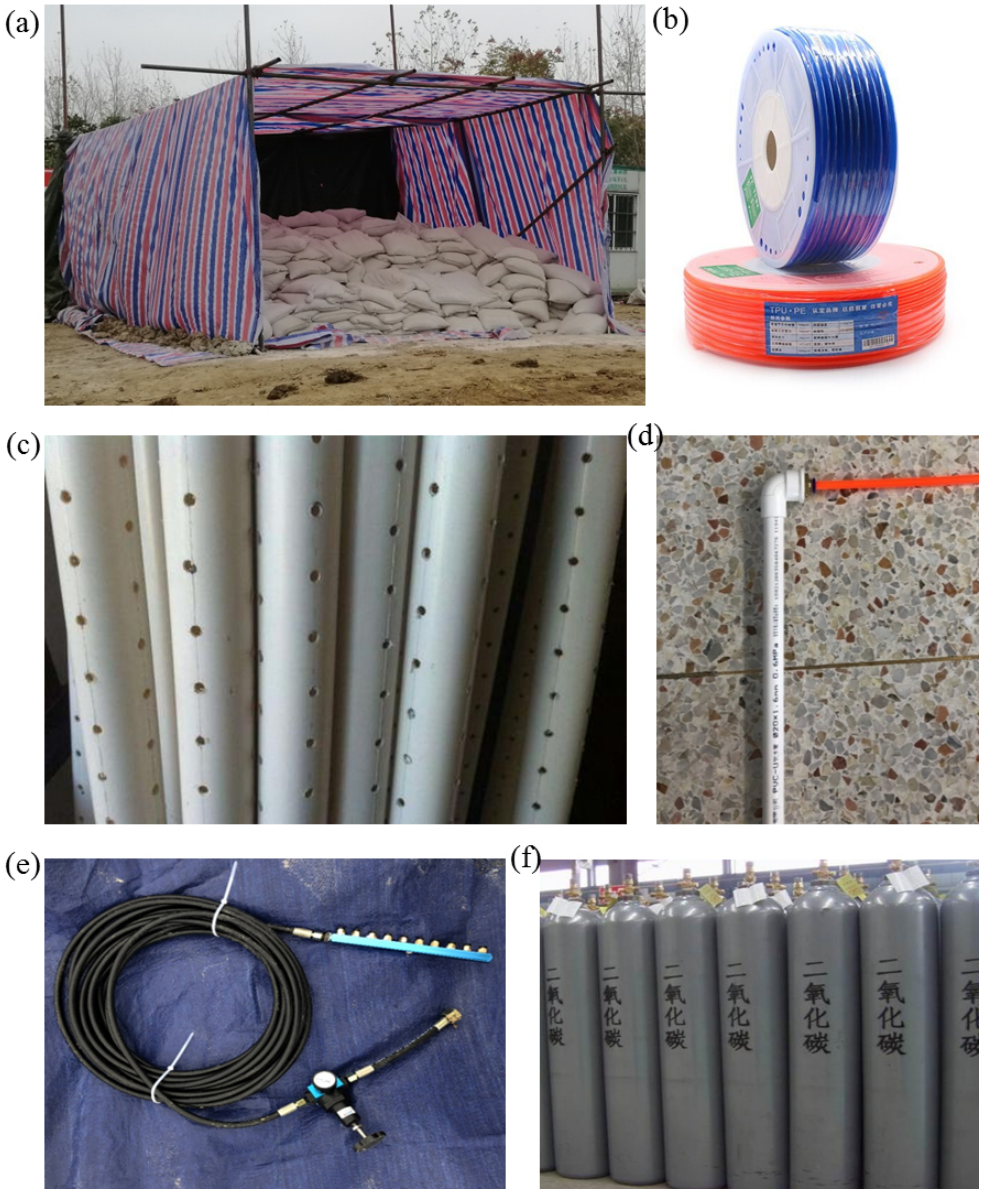

Fig. 2. In-situ experimental materials: (a) industrial MgO; (b) PE pipe; (c) perforated PVC pipe; (d) quick union; (e) high-pressure pipe; and (f) CO2 tank.

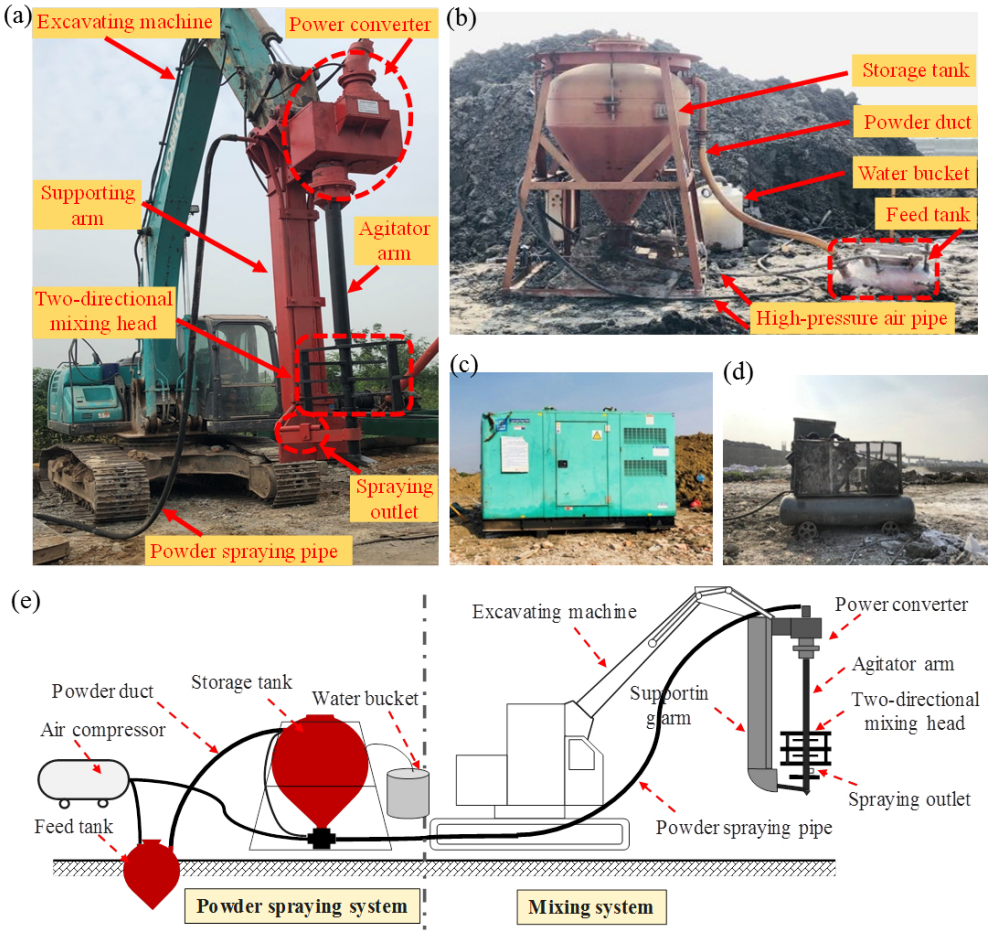

Fig. 3. Main apparatus of in-situ construction: (a) mixing system; (b) binder spraying system; (c) alternator; (d) air compressor; and (e) assembly drawing of system.

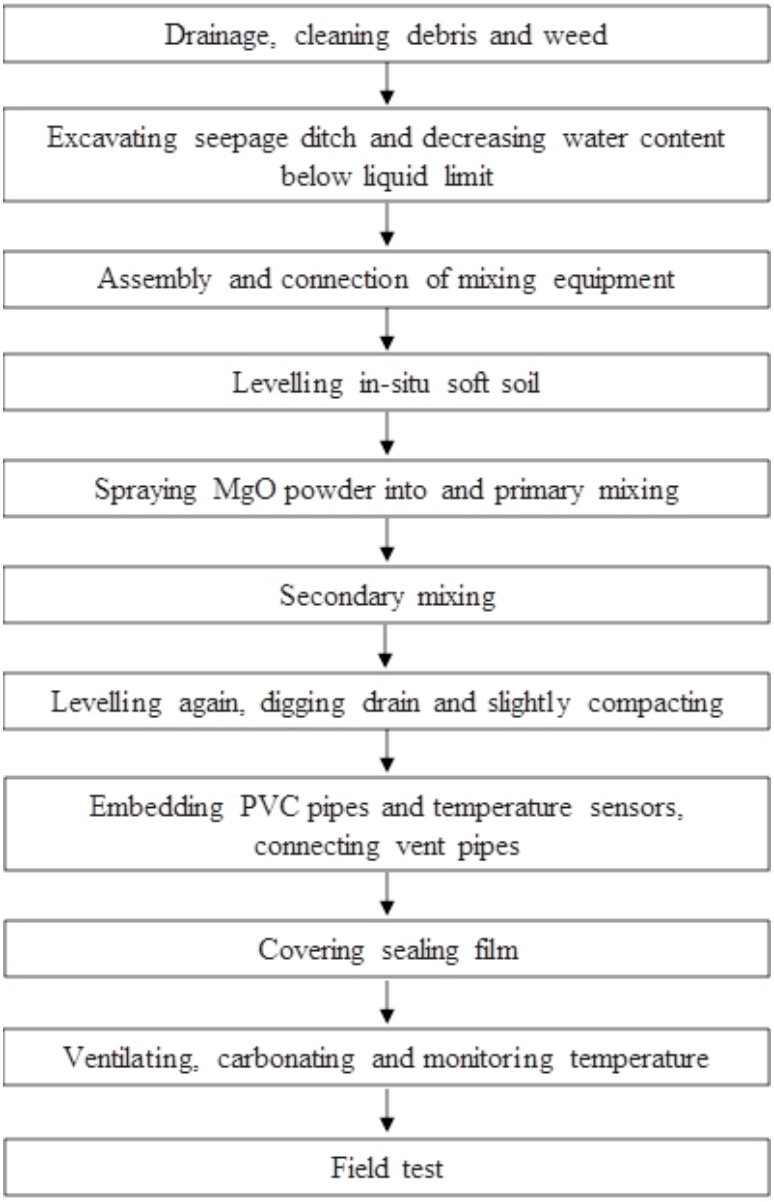

Fig. 4. Flow chart of the construction procedure for the mass carbonation treatment.

Fig. 5. Overview of in-situ construction procedure for mass carbonation treatment: (a) mixing MgO powder; (b) secondary mixing; (c) ditching; (d) inserting PVC; (e) connecting vent pipe; and (f) sealing and carbonating.

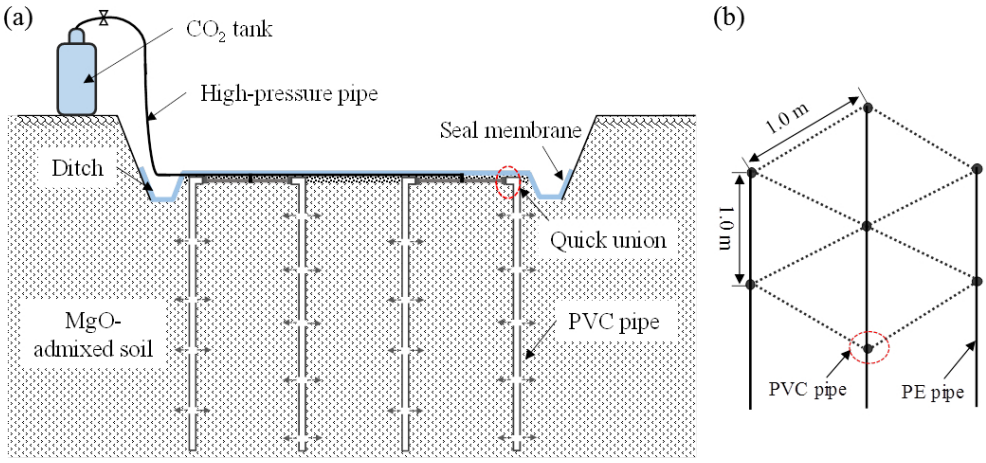

Fig. 6. Arrangement diagram of vent pipes: (a) cross-sectional drawing; and (b) plane drawing.

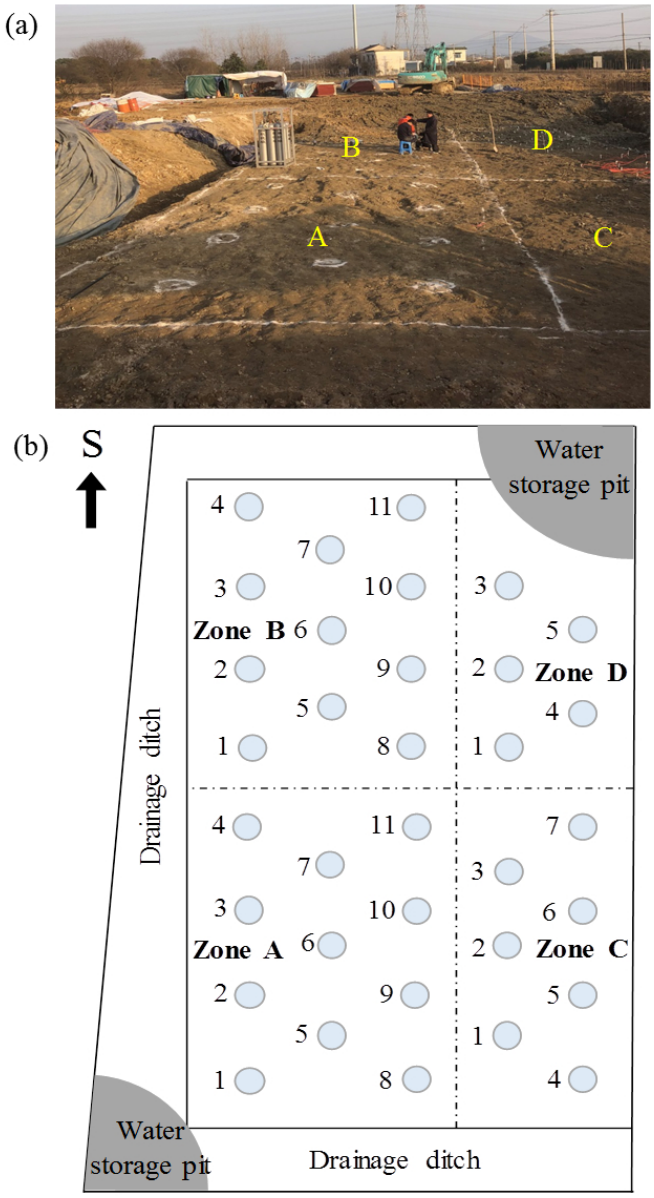

Fig. 7. Layout of field tests: (a) field picture; and (b) diagrammatic figure.

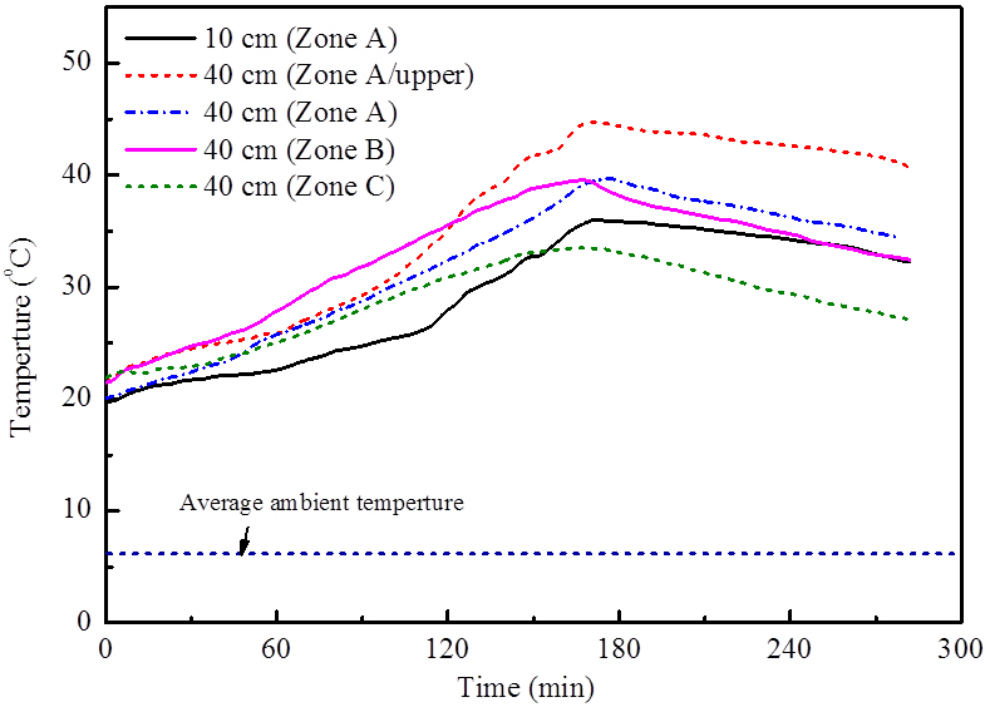

Fig. 8. Variation in temperature of MgO-stabilized soil layers during CO2 ventilation process.

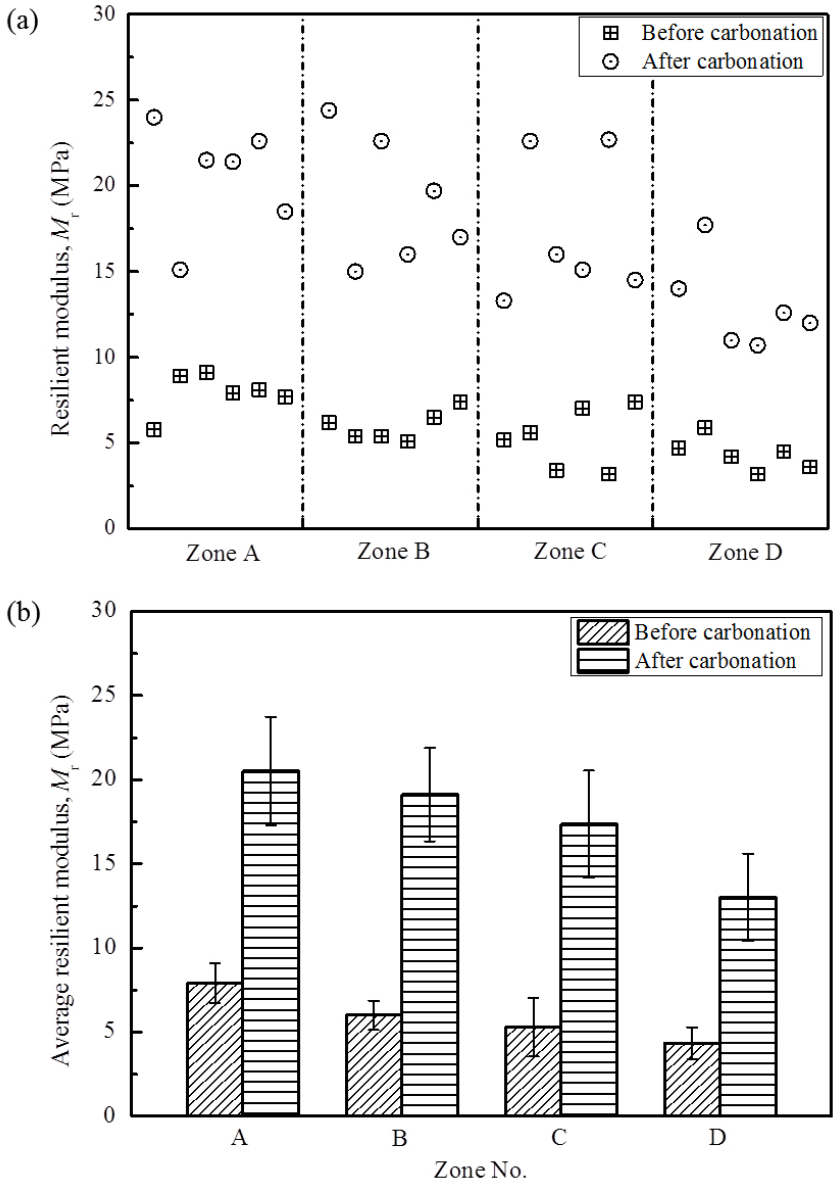

Fig. 9. Dynamic resilient modulus of treated soil layers at different zones ground before and after carbonation: (a) dynamic resilient modulus; and (b) average dynamic resilient modulus.

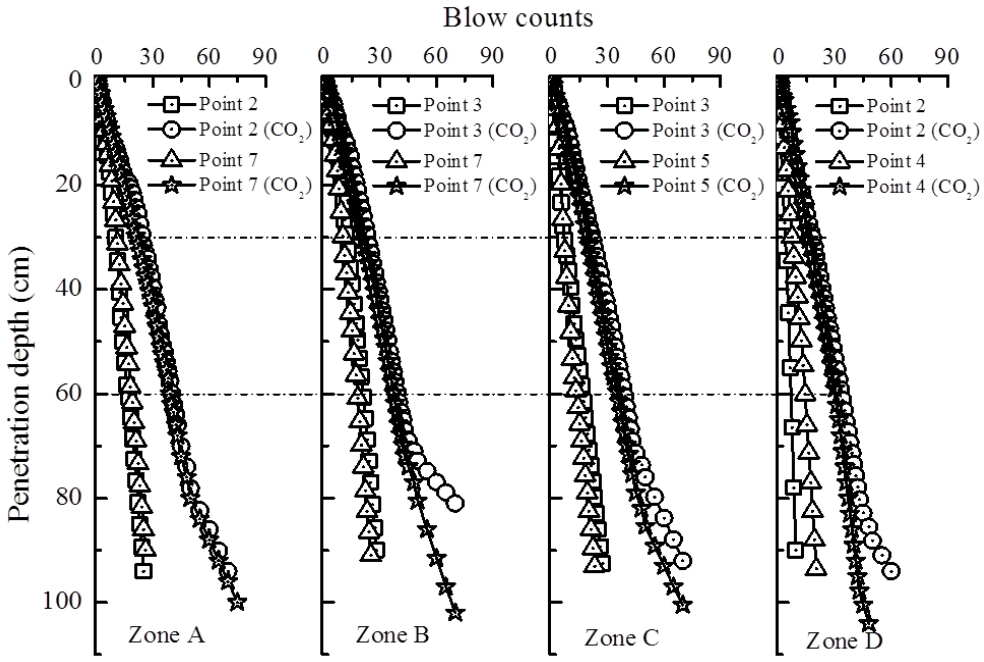

Fig. 10. Variations in blow counts of treated soil layers with penetration depth.

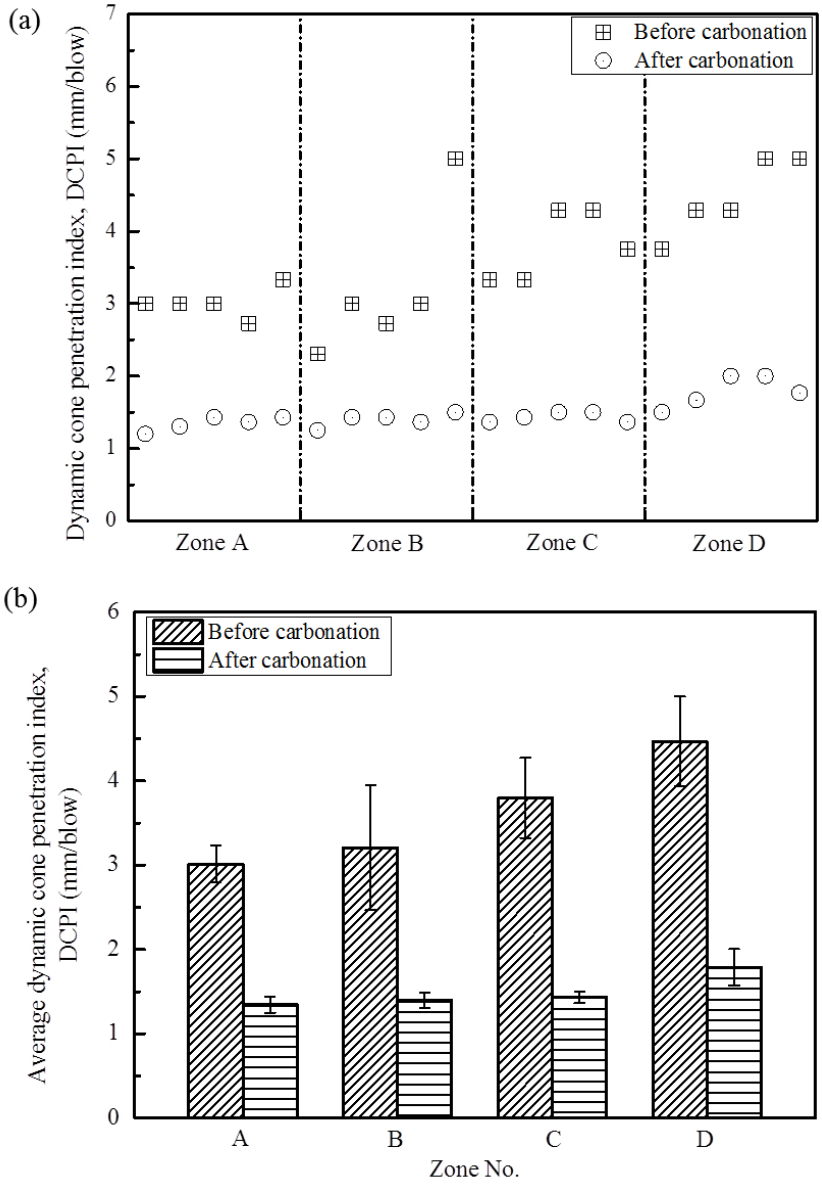

Fig. 11. Variations in dynamic cone penetration index (DCPI) of treated soil layer at different zones: (a) DCPI; and (b) average DCPI.

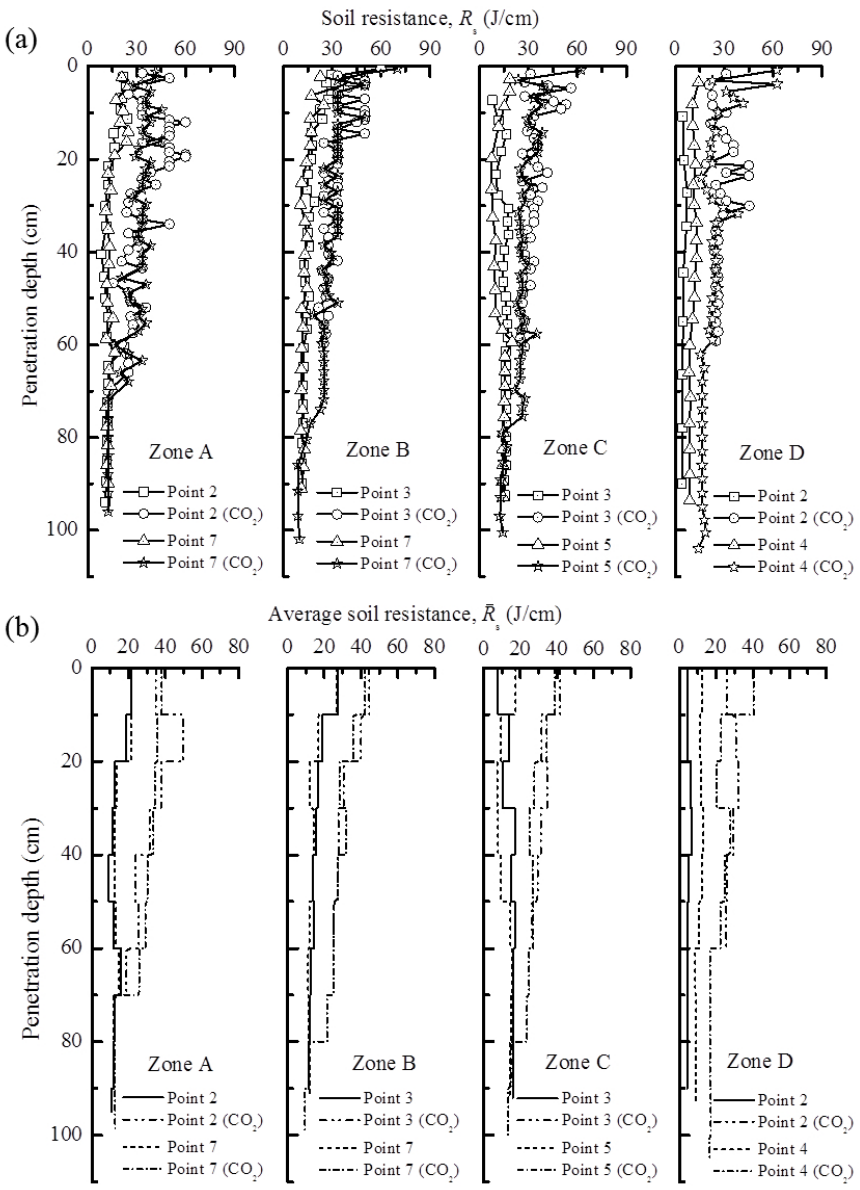

Fig. 12. Variations in the soil resistance of treated soil layers with penetration depth: (a) soil resistance; and (b) average soil resistance.

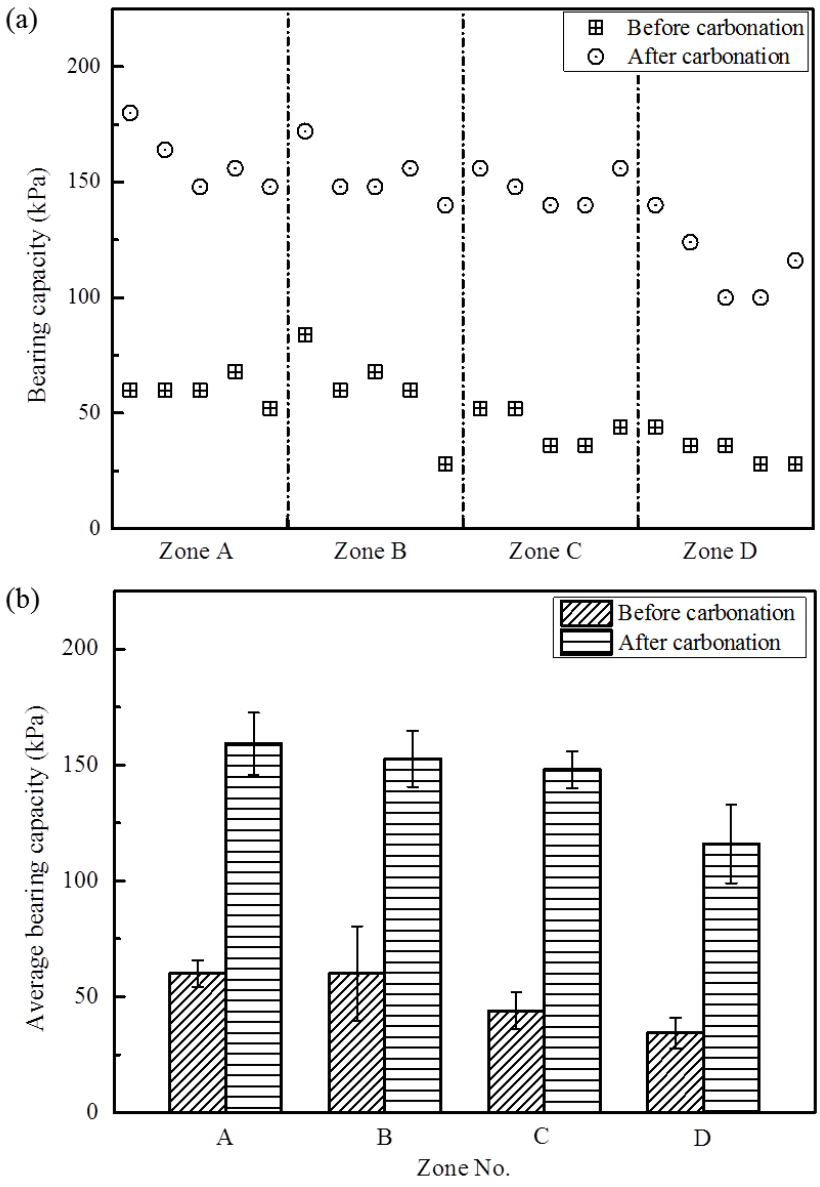

Fig. 13. Variations in bearing capacity of treated soil layers at different zones: (a) bearing capacity; and (b) average bearing capacity.

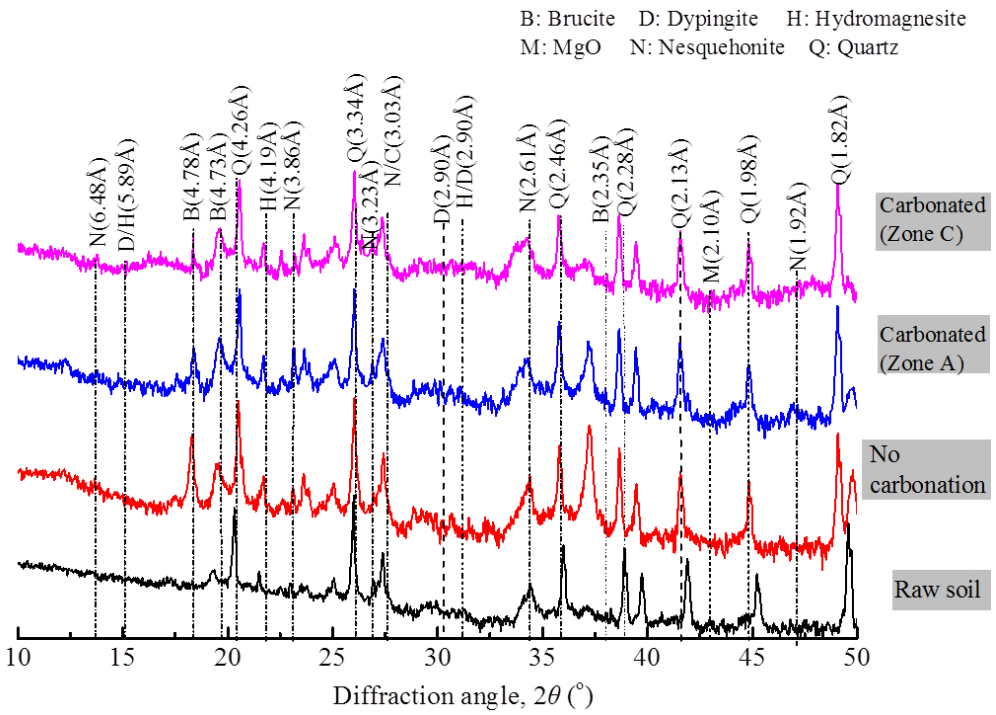

Fig. 14. XRD results of raw soil, MgO-admixed soil and MgO-carbonated soils.

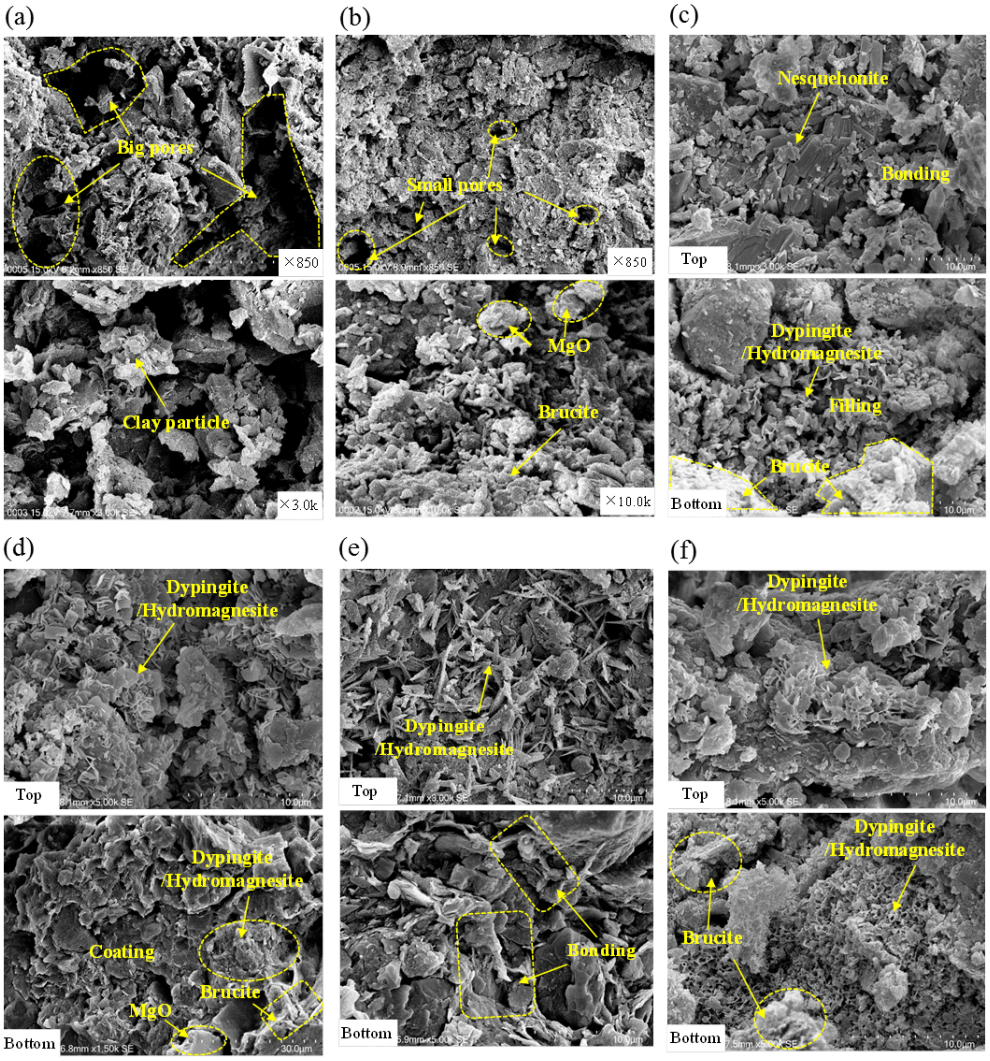

Fig. 15. SEM images of raw soil, MgO-admixed soil and MgO-carbonated soils of different treatment zones: (a) raw soil; (b) MgO-admixed soil; (c) MgO-carbonated soil (zone A); (d) MgO-carbonated soil (zone B); (e) MgO-carbonated soil (zone C); and (f) MgO-carbonated soil (zone D).

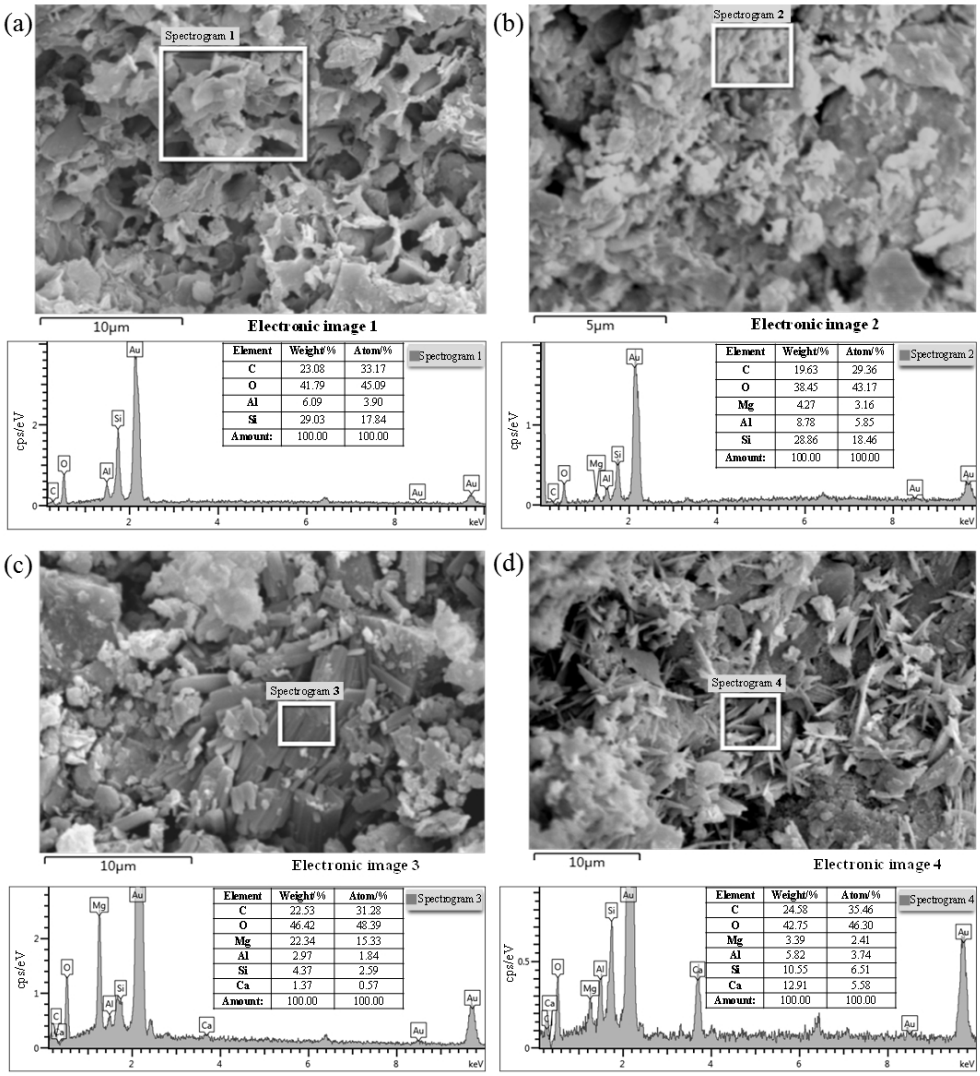

Fig. 16. EDS results of raw soil, MgO-admixed soil and MgO-carbonated soils: (a) Raw soil; (b) MgO-admixed soil; (c) MgO-carbonated soil (zone A); and (d) MgO-carbonated soil (zone C) (Note: the upper part indicates electronic images and the lower part indicates EDS results of designated areas).